JVI Journals.ASM.org

Loss of Cytoskeletal Transport during Egress Critically Attenuates Ectromelia Virus Infection *In Vivo*

Helena Lynn,[a] Jacquelyn Horsington,[a] Lee Kuan Ter,[b] Shuyi Han,[a] Yee Lian Chew,[a] Russell J. Diefenbach,[c] Michael Way,[d] Geeta Chaudhri,[b] Gunasegaran Karupiah,[b] and Timothy P. Newsome[a]

School of Molecular Bioscience, University of Sydney, Sydney, NSW, Australia[a]; John Curtin School of Medical Research, Australian National University, Canberra, ACT, Australia[b]; Centre for Virus Research, The Westmead Millennium Institute, University of Sydney, Westmead, NSW, Australia[c]; and Cancer Research UK, Lincoln's Inn Fields Laboratories, London, United Kingdom[d]

Egress of wrapped virus (WV) to the cell periphery following vaccinia virus (VACV) replication is dependent on interactions with the microtubule motor complex kinesin-1 and is mediated by the viral envelope protein A36. Here we report that ectromelia virus (ECTV), a related orthopoxvirus and the causative agent of mousepox, encodes an A36 homologue (ECTV-Mos-142) that is highly conserved despite a large truncation at the C terminus. Deleting the ECTV A36R gene leads to a reduction in the number of extracellular viruses formed and to a reduced plaque size, consistent with a role in microtubule transport. We also observed a complete loss of virus-associated actin comets, another phenotype dependent on A36 expression during VACV infection. ECTV ΔA36R was severely attenuated when used to infect the normally susceptible BALB/c mouse strain. ECTV ΔA36R replication and spread from the draining lymph nodes to the liver and spleen were significantly reduced in BALB/c mice and in Rag-1-deficient mice, which lack T and B lymphocytes. The dramatic reduction in ECTV ΔA36R titers early during the course of infection was not associated with an augmented immune response. Taken together, these findings demonstrate the critical role that subcellular transport pathways play not only in orthopoxvirus infection in an *in vitro* context but also during orthopoxvirus pathogenesis in a natural host. Furthermore, despite the attenuation of the mutant virus, we found that infection nonetheless induced protective immunity in mice, suggesting that orthopoxvirus vectors with A36 deletions may be considered another safe vaccine alternative.

The crowded, densely packed cytoplasm presents a significant hurdle to the subcellular transport of viruses, both in the translocation of viruses to their site of replication following cell entry and in the subsequent egress of progeny viruses to the cell periphery (16, 18, 29, 69, 70). This hurdle is most acute for large double-stranded DNA (dsDNA) viruses such as those belonging to the orthopoxvirus genus, which includes variola virus (VARV) and ectromelia virus (ECTV), the causative agents of smallpox and mousepox, respectively, and the prototypical orthopoxvirus, vaccinia virus (VACV). These viruses have a complicated replication cycle that has been studied best at the cellular level with VACV. Vaccinia virus replication produces two infectious forms: mature intracellular virus (MV), which has a single membrane and is generated at the so-called virus factory; and wrapped virus (WV), which is derived from MV and acquires an additional double membrane at the *trans*-Golgi network or early endosome compartment (33, 58). While it is apparent that microtubule transport plays a critical role at multiple stages during VACV replication, the stage best characterized at the molecular level is the transport of WV from the *trans*-Golgi network to the cell periphery (27, 32, 57, 75, 76). Once there, WV fuse with the plasma membrane and are released either directly or following the transient activation of actin-based motility (9, 57, 77).

The viral protein A36 (encoded by A36R) is highly conserved across orthopoxviruses and plays an important role in subcellular transport during VACV egress (15, 57, 74). A36 is a type Ib transmembrane protein that is localized to the *trans*-Golgi network and acquired during wrapping of WV at this compartment, and it contains an ~190-residue surface in contact with the cytoplasm (60, 73). Viruses deleted for A36R display a reduction in transport of WV to the cell surface, a phenotype reminiscent of that of cells treated with the microtubule-destabilizing drug nocodazole (14, 15, 27, 31, 57). A key role for A36 is to direct the recruitment of the kinesin-1 anterograde motor complex. This interaction appears to occur via a direct interaction with the kinesin-1 light chain (KLC) and was recently mapped to a bipartite tryptophan motif in A36, at residues 64 and 65 (WE) and residues 97 and 98 (WD) (15, 57, 74), with WD playing the dominant role and WE playing an ancillary role. Conversely, expression of constructs that interfere with kinesin-1 function also inhibits WV egress from the *trans*-Golgi network (57, 65). A simple paradigm that emerges from these findings is that A36 on the surface of WV presents an interaction site for kinesin-1 resulting in transport to the cell periphery. Confounding this paradigm is the viral protein F12, which has also been implicated in the microtubule transport of WV, but recent reports are conflicting regarding the exact function of this protein, and its mechanism of action remains to be clarified (14, 35, 41, 72). A36 also directs a second transport event following delivery of WV to the cell periphery, whereby phosphorylation of two tyrosine residues (residues 112 and 132) initiates a cascade of events leading to recruitment of the Arp2/3 complex beneath extracellular cell-associated WV and to the rapid nucleation of actin filaments (26, 40, 43, 44, 54, 64, 77). Polymerization of actin filaments

Received 24 October 2011 **Accepted** 30 March 2012
Published ahead of print 24 April 2012
Address correspondence to Timothy P. Newsome, tim.newsome@sydney.edu.au.
Supplemental material for this article may be found at http://jvi.asm.org/.

doi:10.1128/JVI.06636-11

TABLE 1 Primers used for constructing plasmids

Gene	Primer name	Primer sequence (5′–3′)
A36R-RA	a36r.rafor	ACCGCGGCCGCCAGATAATGCAGTTTATCAGTGTCG
	a36r.rarev	ACAGGATCCGCTCAATATACGTACTACTAGTTC
A36R-LA	a36r.lafor	AAAAAGCTTCTGTTGAAGTACTTAATGAAGATACC
	a36r.larev	AAAGTCGACCGGATGCTCGAGGTTACAAACATGG
A36R	a36r.for	GGGAGATCTACCATGATGCTGGTACCACTTATCACG
	a36r.rev	TTTGCGGCCGCCGAAAGGATTGGATGAAAGTTAGG
$A36R^{Y112F}$	a36r.mutfor	AGCACGGAACATATTTTCGATAGTGTTGCCGGA
	a36r.mutrev	TCCGGCAACACTATCGAAAATATGTTCCGTGCT
Lifeact	LifeactGFP.for	AAAGATCTACCATGGGTGTCGCAGATTTGATCAAGAAATTCGAAA GCATCTCAAAGGAAGAAGCGGCCGCCAGCAAGGGC
	GFPrev	TTTGGATCCAACTCCAGCAGGACCATGTGA

beneath extracellular WV propels these particles across the surface of the cell, thereby facilitating cell-to-cell spread (13, 75).

Due to the hazards of working with VARV and the unknown host and origin of VACV, ECTV infection in mice has been used extensively as a model for smallpox infection (3, 23). There is a wealth of knowledge on the pathogenesis of ECTV and the murine immune response to infection. Despite this, there is surprisingly little known regarding the cell biology of infection, with research so far delving into such areas as viral subversion of the immune system (42, 66, 67), the ubiquitin proteasome system (34, 78), viral-mediated syncytium formation (22), and preliminary studies on intracellular transport and intercellular spread (2, 4). The high level of conservation between VACV and ECTV genomes affords the opportunity to address the contribution of subcellular transport pathways to virulence in a natural host (8). In the present study, we have demonstrated that both microtubule- and actin-based transport pathways are in operation during ECTV replication. Since A36R is required for these events during VACV infection, we identified an ECTV homologue of A36R, annotated ECTV-Mos-142 or 137.5f (http://poxvirus.org) and referred to henceforth as A36R, that was highly conserved, albeit truncated at the C terminus. Deletion of A36R resulted in ECTV that had a reduction in the appearance of extracellular WV, consistent with reduced microtubule transport, and in the loss of virus-associated actin comets. Both of these phenotypes were rescued by transient expression of ECTV A36R, indicating that these phenotypes were specific for the loss of this protein. Infection of ECTV-susceptible BALB/c mice with ΔA36R virus resulted in drastically attenuated pathogenesis, including a strong reduction in the spread of virus from the site of inoculation and lower viral loads in the major target organs. Virus spread and replication were also significantly curtailed in Rag-1-deficient mice, which lack a functional adaptive immune system. Nonetheless, BALB/c mice that survived ΔA36R infection effectively generated protective antibody and cytotoxic T lymphocyte (CTL) responses and were able to overcome a subsequent lethal challenge with wild-type (WT) ECTV.

MATERIALS AND METHODS

Ethics statement. This study was performed in strict accordance with the recommendations in the Australian code of practice for the care and use of animals for scientific purposes and with the Australian National Health and Medical Research Council guidelines and policies on animal ethics. The protocol was approved by the Animal Ethics and Experimentation Committee of the Australian National University (permit J.IG.75.09).

Cells and viruses. Mammalian cell lines used were HeLa, BSC-1, and NIH 3T3 cells, mouse embryonic fibroblasts (MEFs), and N-Wasp null MEFs (68), and the virus strains were VACV Western Reserve (WR) and ΔA36R (51). The murine cell lines P-815 (H-2d) and YAC-1 were obtained from the American Type Culture Collection (Rockville, MD). The ECTV Moscow strain (ECTV-Mos/WT ECTV; ATCC VR1374) was a gift from R. M. Buller, St. Louis University School of Medicine. Cells were grown in Gibco Dulbecco's modified Eagle Medium (DMEM; Invitrogen) supplemented with 5% fetal bovine serum (FBS), 292 μg/ml L-glutamine, 100 units/ml penicillin, and 100 μg/ml streptomycin and incubated at 37°C in a 5% CO_2 atmosphere. For infection, virus was diluted in DMEM not supplemented with FBS and applied to phosphate-buffered saline (PBS)-washed cells. Cells were incubated at 37°C with a 5% CO_2 atmosphere for 1 h before being recovered with fresh growth medium. For plaque assays, confluent BSC-1 monolayers were infected as described above, but instead of recovery with fresh growth medium, they were overlaid with Gibco modified Eagle medium (MEM; Invitrogen) supplemented with 292 μg/ml L-glutamine, 100 units/ml penicillin, 100 μg/ml streptomycin, and 1.5% carboxymethyl cellulose (CMC). Plaques were allowed to form for 5 days before examination.

Plasmid construction. To construct a recombination cassette for deletion of A36R, regions of approximately 900 bp of ECTV Mos genomic DNA flanking the A36R gene locus were amplified with primers a36r.ra.for and a36r.ra.rev for the right flanking region and a36r.la.for and a36r.la.rev for the left flanking region (Table 1). PCR products were gel purified with a gel extraction kit (Promega), digested, and ligated into a plasmid vector flanking monomeric red fluorescent protein (mRFP) and a guanosine phosphotransferase (GPT) selection marker.

To construct a plasmid encoding the ECTV A36 protein fused N-terminally to green fluorescent protein (GFP), the A36R gene was amplified from ECTV Mos genomic DNA with primers a36r.for and a36r.rev. PCR products were gel purified with a gel extraction kit (Promega) and digested with BglII and NotI before ligation into a plasmid vector containing the GFP gene under the control of a synthetic viral early/late promoter (pE/liter) (5, 57). A plasmid encoding ECTV $A36^{Y112F}$ fused to GFP was constructed in the same way, excepting the initial PCR amplification, which instead was a two-step fusion PCR. The first step involved amplification of ECTV genomic DNA with primer pairs a36r.for-a36r.mutrev and a36r.mutfor-a36r.rev, which each amplified half of A36R. These PCR products were used as the template for a second step of amplification with primers a36r.for and a36r.rev, resulting in a full-length A36R gene product incorporating a Tyr-to-Phe mutation at site 112. VACV A36R-GFP plasmid was constructed as described previously (1), with wild-type A36R rather than A36R-YdF.

A plasmid encoding Lifeact, a 17-amino-acid peptide that binds to filamentous actin (56), fused N-terminally to GFP under the control of pE/L, was constructed in a similar process to that described above. However, the sequence of Lifeact was incorporated into the synthesized primer LifeactGFP.for, which was used with the GFPrev primer on a plasmid template of GFP to generate a PCR product spanning all of the GFP se-

quence. This PCR product was digested with BglII and NotI, purified with a QiaexII gel extraction kit (Qiagen), and ligated into a pE/L GFP vector.

Transient expression of constructs. HeLa or BSC-1 cells grown to 70% confluence were infected for 1 h and recovered with fresh growth medium for an additional 1 h before being transfected with ECTV A36R-GFP, ECTV A36R^{Y112F}-GFP, or VACV A36R-GFP by a standard protocol using Lipofectamine 2000 (Invitrogen).

Recombinant virus construction. HeLa cells grown to 70% confluence were infected with ECTV Mos and transfected with the recombination cassette by a standard protocol using Lipofectamine 2000 (Invitrogen). Cells were scraped at 24 h postinfection (hpi) to allow for homologous recombination between genomic DNA and the recombination cassette and then were lysed by freeze-thawing. Plaque assays were carried out with the addition of GPT selection medium (25 μg/ml mycophenolic acid [MPA], 250 μg/ml xanthine, 15 μg/ml hypoxanthine) in the overlay. Plaques able to grow under GPT selection that displayed mRFP fluorescence were purified and verified as ΔA36R virus by sequencing.

Antibodies and fluorescent chemicals. The primary antibodies used in this study were: anti-A36 (60), anti-B5 (9), anti-β-actin (Sigma-Aldrich), anti-kinesin-1 heavy chain (anti-KHC) (H-50; Santa Cruz Biotechnology), anti-phosphotyrosine (4G10; Chemicon), and anti-mRFP (Chemicon). Anti-A36-Y112 was raised against the phosphorylated peptide corresponding to residues 105 to 119 of VACV A36 (APSTEHIpYDS VAGST) and purified as described previously (43), but it is not dependent on phosphorylation of tyrosine 112 of A36. The secondary antibodies used in this study were as follows (all from Invitrogen): Alexa Fluor 568-conjugated goat anti-mouse IgG, Alexa Fluor 488-conjugated goat anti-mouse IgG, Alexa Fluor 350-conjugated goat anti-mouse IgG, Alexa Fluor 568-conjugated goat anti-rabbit IgG, Alexa Fluor 488-conjugated goat anti-rabbit IgG, Alexa Fluor 488-conjugated goat anti-rat IgG, Alexa Fluor 350-conjugated goat anti-rat IgG, Alexa Fluor 568-conjugated goat anti-rat IgG, anti-rabbit–horseradish peroxidase (HRP), and anti-mouse–HRP. Fluorescent chemicals used were as follows: DAPI (4′,6-diamidino-2-phenylindole; Sigma-Aldrich) (1 μg/ml), Alexa Fluor 488-phalloidin, and Alexa Fluor 568-phalloidin (Invitrogen) (1:300 dilution).

Immunofluorescence analyses. Cells were grown on glass coverslips, infected with appropriate viruses, and fixed at 8 hpi (VACV) or 24 hpi (ECTV) (unless otherwise stated) with 3% paraformaldehyde (PFA) in cytoskeletal buffer (CB) [10 mM 2-(*N*-morpholino)ethanesulfonic acid (MES) buffer, 0.15 M NaCl, 5 mM EGTA, 5 mM $MgCl_2$, 50 mM glucose, pH 6.1] for 10 min at room temperature. Before staining, cells were either permeabilized with 0.1% Triton X-100 in CB or not permeabilized, depending on whether the protein of interest was intracellular or extracellular. Cells were blocked in blocking buffer (1% bovine serum albumin [BSA] and 2% FBS in CB) for 20 min and then incubated for 40 min with suitable primary antibodies diluted in blocking buffer. After three washes with PBS, secondary antibodies diluted in blocking buffer were applied to cells for 20 min. The coverslips were mounted on a glass slide with 0.3 to 1% (wt/vol) *p*-phenylenediamine (Sigma-Aldrich) in Mowiol mounting medium (10% [wt/vol] polyvinyl alcohol 4-88 [Sigma-Aldrich], 25% [wt/vol] glycerol, 0.1 M Tris, pH 8.5). Fluorescence and phase-contrast microscopy was performed with an Olympus microscope BX51 with filter sets 31001, 31002, and 31013v2 (Chroma), and resulting images were analyzed with Photoshop CS3 (Adobe).

Immunoblot analysis. Cells were harvested in sodium dodecyl sulfate (SDS)-reducing sample buffer (62.5 mM Tris-HCl, 0.25 M glycerol, 2% SDS, 0.01% [wt/vol] bromophenol blue, 12.5% [vol/vol] β-mercaptoethanol) and boiled at 95°C for 5 min. Proteins were separated by SDS-polyacrylamide gel electrophoresis (SDS-PAGE) (resolving gel of 10% acrylamide-Bis solution [37.5:1], 0.375 M Tris-HCl, pH 8.8, 0.1% [wt/vol] SDS, 0.1% ammonium persulfate (APS), and 0.1% *N*,*N*,*N*′,*N*′-tetramethylethylenediamine [TEMED]; stacking gel of 4% to 30% acrylamide-Bis solution [37.5:1], 0.375 M Tris-HCl, pH 6.8, 0.1% [wt/vol] SDS, 0.1% APS, and 0.1% TEMED). Resolved proteins from SDS-PAGE were transferred to nitrocellulose membranes (Hybond-C Extra; Amersham Biosciences) and probed with primary antibodies diluted in PBST-milk (5% [wt/vol] skim milk in PBS with 0.1% Tween 20). The membrane was washed three times in PBST-milk and probed with secondary antibodies conjugated with horseradish peroxidase. Immunoreactive protein bands were visualized with ECL Western blotting reagent (GE Health).

Live-cell microscopy. Glass-bottom dishes (35 mm; Mat Tek) were coated in 5 μg/cm^2 fibronectin (Sigma-Aldrich) for 2 h before HeLa cells were seeded and grown to 70% confluence. Cells were infected for 1 h, rescued, and transfected with pE/L Lifeact-GFP 6 h prior to imaging. At either 8 to 10 hpi (VACV) or 24 to 26 hpi (ECTV), cells were imaged on an Olympus FV1000 confocal microscope with a 488-nm laser line. Resulting movies were processed with the Manual Tracking plug-in in Image J.

Mouse experiments. Inbred, specific-pathogen-free female BALB/cAnNCrl (BALB/c), C57BL/6J wild-type, and Rag-1-deficient B6.129S7-Rag1^{tm1Mom}/J (B6.Rag-1$^{-/-}$) (39) mice on a C57BL/6J background at 6 to 8 weeks of age were obtained from the Australian National University Bioscience Services (Canberra, ACT, Australia). Groups of female BALB/c mice were infected subcutaneously in the left hind leg with 10^2, 10^3, or 10^4 PFU ECTV or ECTV ΔA36R and monitored for survival and clinical signs of disease for 33 days. Separate groups of infected mice were euthanized at 5 and 8 days postinfection (dpi). Rag-1$^{-/-}$ mice were inoculated with 10^3 PFU virus and also sacrificed at 5 and 8 dpi for determination of viral titers in organs. Viral loads in livers, spleens, and lymph nodes were quantified by viral plaque assay on BSC-1 cell monolayers as described previously (7) and are expressed as $\log_{10}$ PFU per gram of tissue or per lymph node. At 28 dpi, all surviving BALB/c mice infected with ECTV ΔA36R from the first group were bled and then challenged with a lethal dose of 10^4 PFU ECTV by the subcutaneous route on day 33. Eight days later, mice were sacrificed, and anti-ECTV antibody in serum and virus loads in the spleen, liver, and lymph nodes were measured.

ELISA. Serum samples were assayed by enzyme-linked immunosorbent assay (ELISA) for total ECTV-specific IgG as described earlier (47). Briefly, U-bottom 96-well plates (Immulon 2; Dynatech Lab Inc., Alexandria, VA) were coated with purified ECTV. Sera were assayed at a 1:200 dilution, and ECTV-specific antibody was detected using horseradish peroxidase-conjugated goat anti-mouse IgG (Southern Biotechnology Associates, Birmingham, AL) and color developed with TMB One-Step substrate (Dako Cytomation, Carpinteria, CA).

Plaque reduction neutralization test. The plaque reduction neutralization test, used to determine the neutralizing activity of antibody to ECTV present in serum samples, has been described previously (47). Serial dilutions of sera, starting at a 1:50 dilution, were incubated with 100 PFU of ECTV for 1 h before being added to wells of BSC-1 cell monolayers. The neutralization titer was taken as the reciprocal of the dilution of serum that caused a 50% reduction in the number of virus plaques.

CTL and NK cell assays. Cytotoxic T lymphocyte (CTL) and natural killer (NK) cell assays were performed as described elsewhere (7, 36). To measure *ex vivo* CTL responses, spleen cells from infected animals were assessed for the ability to kill ^{51}Cr-labeled virus-infected or uninfected syngeneic P815 target cells over a 6-h culture period. To assess NK cell activity *ex vivo*, spleen cells from infected or uninfected BALB/c and C57BL/6 mice were cultured with ^{51}Cr-labeled YAC-1 target cells for 4 h, and the radioactivity in the supernatant was measured in a TopCount NXT scintillation counter.

RESULTS

Microtubule- and actin-based transport is active during ECTV infection. Orthopoxvirus infection results in the formation of highly compartmentalized replication centers during productive infection. These replication centers can be distinguished using a combination of histological markers and stains. For example, the virus factory is positive for DNA stains such as DAPI and for viral markers, including p14 (A27) (62), but is negative for WV markers A36, A33, A34, and B5, which localize to the *trans*-Golgi network, where MV are wrapped to form WV (60, 73). Using a com-

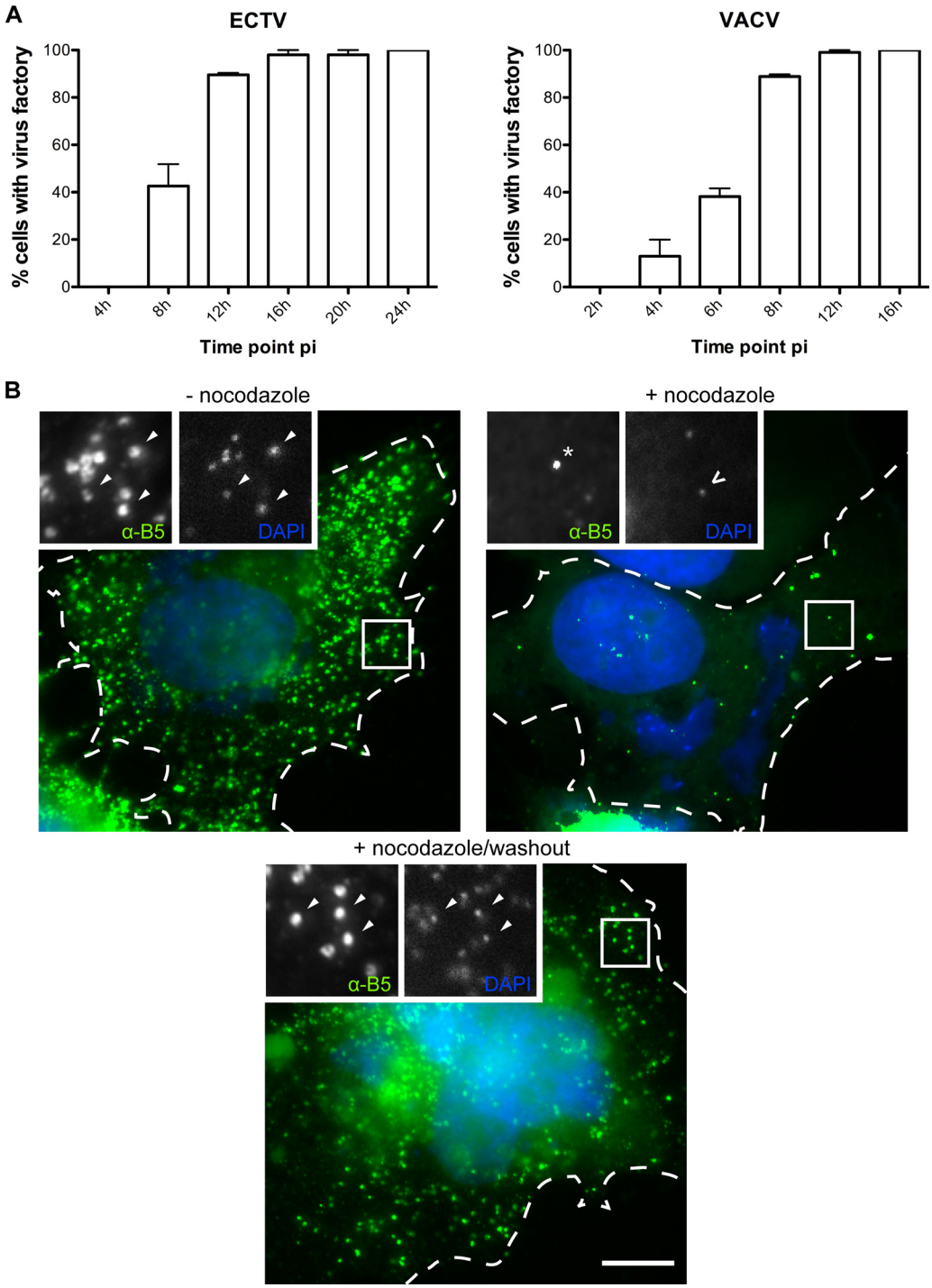

FIG 1 ECTV utilizes microtubules for egress. (A) BSC-1 cells were infected with ECTV or VACV at a multiplicity of infection (MOI) of 1 and fixed at the indicated time points. Cells were stained with DAPI and assessed for the presence of a virus factory ($n = 50$ per time point, in duplicate). The percentage of virus factory-containing cells was calculated. Error bars indicate standard errors. (B) HeLa cells were infected with ECTV, and at 8 hpi, 33 μM nocodazole (Sigma) was added to wells and the cells either fixed 16 h later or washed three times in cell growth medium as a nocodazole washout control. Washout controls were allowed to incubate for an additional 24 h postwashout before being fixed. Nonpermeabilized cells (NPC) were stained for immunofluorescence assays with anti-B5 (green) and DAPI (blue). Arrowheads indicate wrapped virus, the asterisk indicates a B5-positive vesicle, the chevron indicates an MV, and the dotted line indicates the cell periphery, as determined by phase-contrast microscopy.

bination of stains and antibodies specific to VACV proteins found also to cross-react to ECTV proteins, we analyzed ECTV-infected BSC-1 cells at various time points postinfection. Unlike the case for VACV-infected cells, we identified the formation of a virus factory at approximately 4 to 8 hpi (Fig. 1A). B5 expression was initiated at approximately the same time and was generally concentrated at a collapsed *trans*-Golgi network that was localized adjacent to the nucleus (data not shown, but see Fig. 2C). Overall,

ECTV infection closely resembles VACV infection, although it is approximately 1.5-fold slower, and this was found to be the case in multiple cell types, including murine cells (MEFs and NIH 3T3) (data not shown). Hence, ECTV infection faces a similar transport hurdle of delivery of WV from the perinuclear *trans*-Golgi network to the cell periphery. Since this transport step is dependent on microtubule-dependent transport in VACV replication, we tested whether the appearance of extracellular WV required an intact microtubule cytoskeleton. Treatment of infected cells with nocodazole, an agent that interferes with microtubule polymerization, drastically reduced the appearance of WV at the cell surface, confirming that similar to the case for VACV replication, ECTV requires microtubule transport (Fig. 1B). We also localized the kinesin-1 heavy chain (KHC) of the kinesin-1 motor complex to WV particles, suggesting that the mechanism of microtubule transport is also conserved (see Fig. 6B). Previous reports have demonstrated that ECTV also undergoes actin-based transport by the stimulation of the nucleation of actin filaments beneath extracellular WV (2). We observed actin comets in approximately 65% of ECTV-infected BSC-1 cells at 16 hpi, compared to approximately 50% of VACV-infected cells at 8 hpi, which is consistent with the delayed ECTV replication cycle (Fig. 2A and B). Induction of actin-based motility was robust and was observed in multiple cell types, including murine cells (data not shown).

Actin-based motility of VACV is dependent on recruitment of N-Wasp to phosphorylated tyrosines on A36 (via the adaptor proteins Nck, Grb2, and WIP), which then stimulates activity of the Arp2/3 complex (26, 40, 43, 44, 54, 64, 77). We first observed, through immunofluorescence analysis of ECTV-infected cells, that phosphorylated tyrosine localized to actin comets (Fig. 2D). We therefore tested whether N-Wasp was required for ECTV-induced actin-based motility. Infection of N-Wasp knockout MEFs resulted in cells bereft of virus-associated actin comets, a phenotype rescued by transient expression of GFP-tagged N-Wasp (Fig. 2E). Taken together, these results demonstrate that in addition to high conservation at the genomic level, the replication of ECTV is highly conserved with that of VACV at the cellular level, although it is substantially slower. Like that of VACV, replication of ECTV includes transport of WV that appears to be dependent on kinesin-1-mediated microtubule transport and N-Wasp-dependent actin-based motility.

ECTV encodes a homologue of VACV protein A36. The WV-specific viral transmembrane protein A36 is a critical mediator of both actin-based (25) and microtubule-based (15, 57, 74) transport of VACV. We searched the ECTV (Moscow) genome for a homologue of A36 that might be responsible for subcellular transport of WV during ECTV replication. We identified the ECTV open reading frame (ORF) 137.5f as a candidate A36R homologue, consistent with previous findings (8). ECTV A36R resides at a conserved genomic locus and encodes a hypothetical protein of 160 residues with 92% amino acid identity with the first 157 residues of VACV A36 (Fig. 3A). Homology is lost at position 155 of ECTV A36, which appears to be truncated at the C terminus. Despite the predicted C-terminal truncation, the regions critical for actin-based motility (Tyr 112) (25) and the dominant interaction with kinesin-1 (WD [residues 97 and 98]) are conserved (15, 74). The region critical for the ancillary interaction, i.e., residues 64 and 65 (WE) in VACV A36, has an amino acid substitution resulting in a second WD motif in ECTV A36. Using antiserum raised against a peptide corresponding to residues 105 to 119 of VACV A36, we confirmed that ECTV A36 was expressed during ECTV infection, beginning at approximately 8 hpi. ECTV A36 runs at a molecular mass of approximately 32 kDa and is thus smaller than VACV A36, which runs at 43 to 50 kDa (51) (Fig. 3B). Although both proteins run considerably above their predicted molecular masses, the discrepancy is consistent with the deletion in the 3′ end of the ECTV A36R ORF. ECTV A36 also produced a visible band in the presence of cytosine arabinoside (AraC), an inhibitor of DNA replication and late gene expression, which indicates that like VACV A36, ECTV A36 has an early component to its expression (Fig. 3B) (51). Immunofluorescence analysis of ECTV-infected cells demonstrated that A36 localized to the *trans*-Golgi network and colocalized with B5 at single virus particles, consistent with WV labeling (Fig. 2C).

Deletion of A36R results in defective subcellular transport. Since ECTV A36R appeared to be a homologue of VACV A36, based on sequence conservation, expression, and localization, we sought to demonstrate that ECTV A36R is also required for actin- and microtubule-based motility. We generated a plasmid construct designed to replace the A36R open reading frame with selectable and screenable markers. Using this construct, we selected for recombinant virus able to replicate in the presence of GPT selection medium and expressing mRFP from an artificial synthetic early/late promoter. The integrity of the ΔA36R recombinant virus was tested by PCR analysis of genomic DNA (Fig. 4A) and sequencing across the insertion site (data not shown). We confirmed that A36R expression was not detectable in ECTV ΔA36R-infected lysates by immunoblotting (Fig. 4B) and in ECTV ΔA36R-infected cells by immunofluorescence assays (Fig. 4C).

To analyze the replication dynamics and spread of ECTV ΔA36R, we performed WV release assays and plaque assays. There was a severe reduction in infectious virus release during replication of ECTV ΔA36R, although the overall production of infectious virus was unaffected (Fig. 5A and B). The plaque size of ECTV ΔA36R was also greatly reduced compared to that of the parental strain (Fig. 5C and D). Since reductions in plaque size and virus release are consistent with compromised subcellular transport, we next examined ECTV ΔA36R-infected cells by immunofluorescence for the hallmarks of actin- and microtubule-based transport. Loss of A36R resulted in a reduction in the appearance of extracellular WV, and those that reached the cell surface were confined to central regions of the cell, where the *trans*-Golgi network lies in close proximity to the plasma membrane (Fig. 6A). Virus particles no longer colocalized with KHC, consistent with abrogated microtubule-dependent transport (Fig. 6B). WV that did reach the cell surface were not associated with actin comets (Fig. 6C). To confirm that these phenotypes were due specifically to the loss of A36 expression, we were able to rescue transport by the transient expression of GFP-tagged ECTV A36R and A36R-Y112F. While both constructs were able to rescue the motility of WV to the cell surface (Fig. 7A), only A36R-GFP, not A36R-Y112F-GFP, was able to rescue actin-based motility (Fig. 7B). This is consistent with previous findings made with VACV, in which mutation of the critical Tyr 112 to Phe abrogates actin-based motility (26). In summary, ECTV A36 is a functional homologue of VACV A36 and is required for efficient WV intracellular transport and actin-based motility during ECTV infection.

We observed that actin comets that localized to extracellular WV during ECTV infection had a divergent morphology, i.e., on

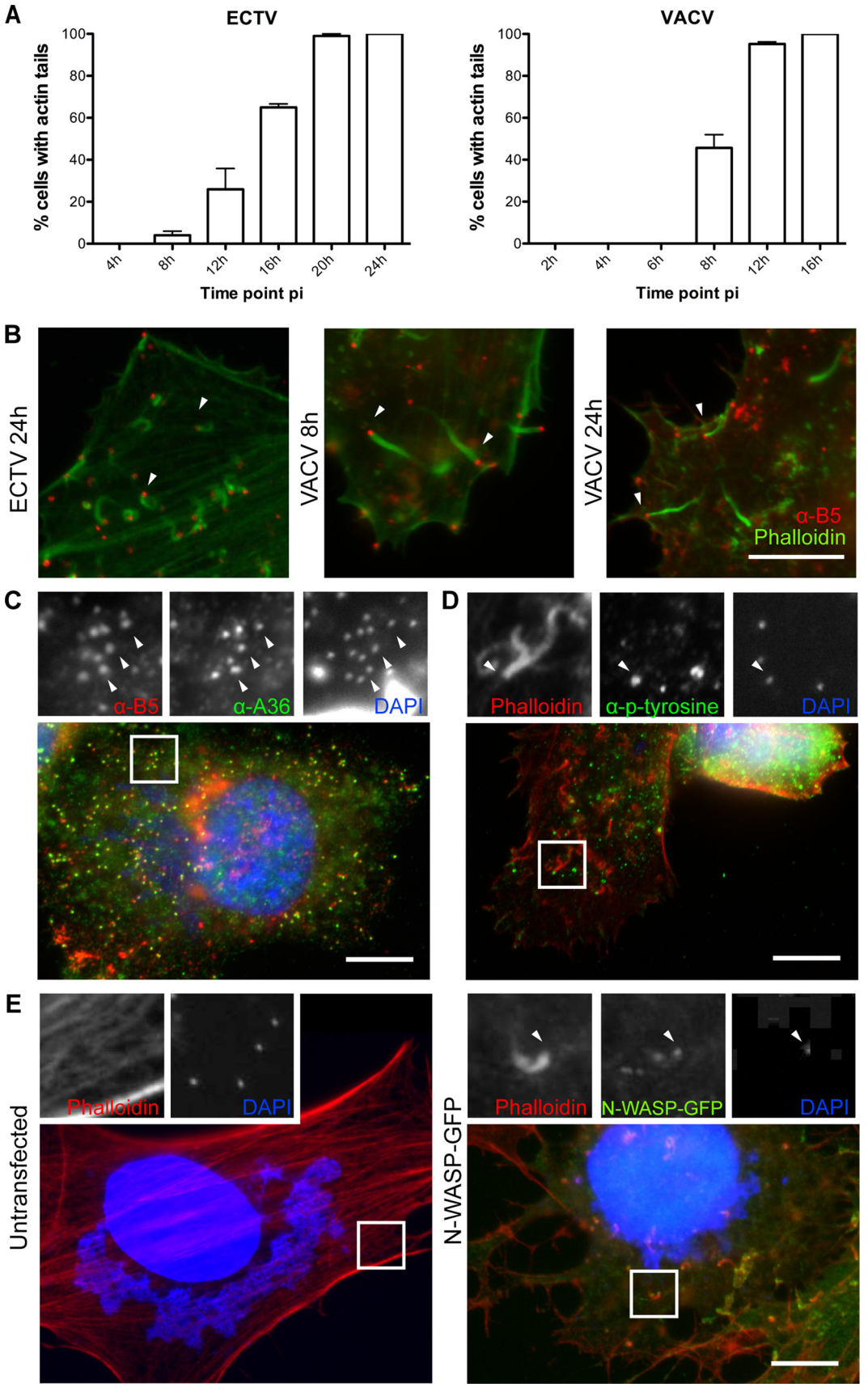
A
ECTV
% cells with actin tails
100
80
60
40
20
0
4h
8h
12h
16h
20h
24h
Time point pi
VACV
% cells with actin tails
100
80
60
40
20
0
2h
4h
6h
8h
12h
16h
Time point pi
B
ECTV 24h
VACV 8h
VACV 24h
α-B5
Phalloidin
C
α-B5
α-A36
DAPI
D
Phalloidin
α-p-tyrosine
DAPI
E
Untransfected
Phalloidin
DAPI
N-WASP-GFP
Phalloidin
N-WASP-GFP
DAPI

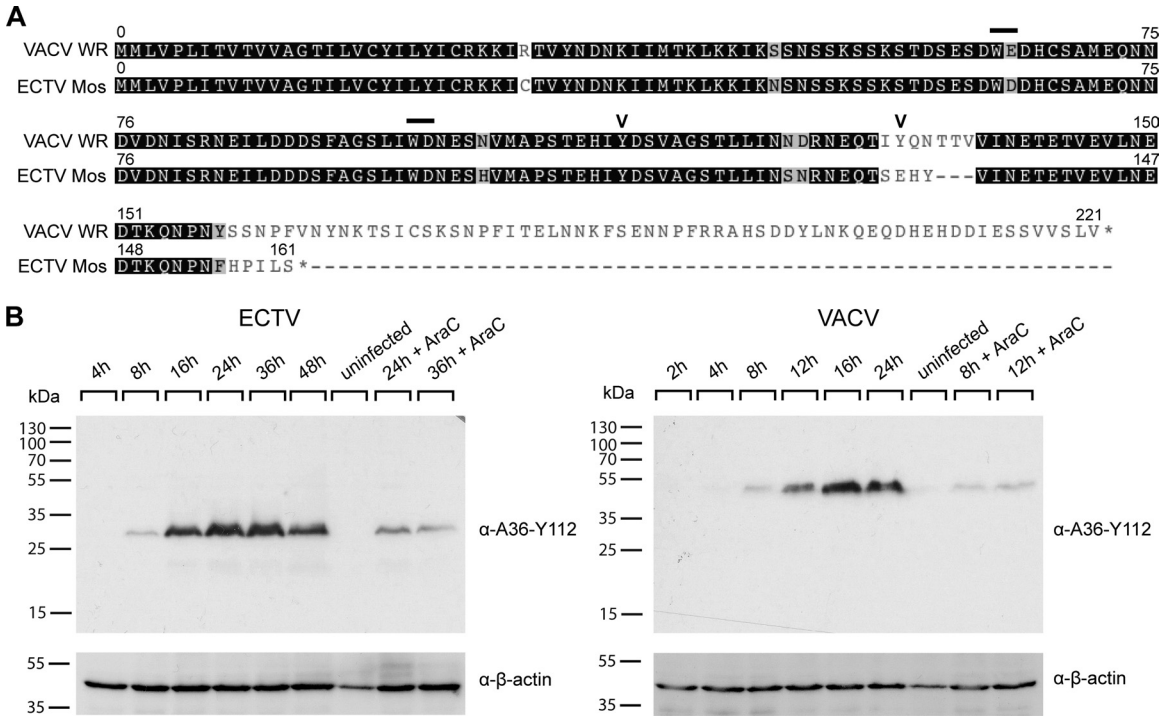

FIG 3 ECTV carries a highly conserved homologue of A36R. (A) Translations of the A36R open reading frames in ECTV Mos (GenBank accession no. AF012825) and VACV WR (GenBank accession no. AY243312), obtained from http://poxvirus.org and aligned in Geneious 5.4.4 (Biomatters Ltd.). Bars represent bipartite tryptophan domains for binding of kinesin-1 and microtubule-based motility. Chevrons represent tyrosine phosphorylation sites for actin-based motility. (B) BSC-1 cells were infected with ECTV or VACV at an MOI of 1 in the absence or presence of 40 μg/ml AraC (Sigma) at the indicated time points. Cell lysates were separated by SDS-PAGE and transferred to nitrocellulose membranes for immunoblotting with anti-A36-Y112, detecting ECTV or VACV A36. Immunoblots were also probed with anti-β-actin as a loading control. Molecular size markers are indicated on the left.

average, they were shorter (1.59 μm for ECTV and 2.88 μm for VACV) (Fig. 8A), and this difference was found to be statistically significant ($P < 0.0001$; unpaired t test). The difference in actin comet morphology could be due to differences between the viral initiators of actin polymerization (ECTV A36 and VACV A36), in particular the C-terminal truncation, differences in other viral proteins, or differences in the time point at which actin-based motility was visualized due to the delayed ECTV replication cycle. We determined that the distinct morphologies of ECTV- and VACV-induced actin comets were not due to delayed replication dynamics, as VACV-infected cells at 24 hpi retained the VACV-like morphology (Fig. 2B). We therefore focused on testing the former hypotheses. We examined WV-associated actin comets in VACV ΔA36R- and ECTV ΔA36R-infected cells transiently rescued with GFP-tagged VACV A36 and ECTV A36. Experiments demonstrated that ECTV ΔA36R produced statistically shorter tails than those of VACV ΔA36R when rescued with either GFP-tagged VACV A36 or ECTV A36 (unpaired t test; $P = 0.0006$ and $P = 0.0041$, respectively) (Fig. 8A). This verified that the difference in WV-associated actin comet morphology is inherent to the background of the virus and not the identity of the viral initiator.

Live-cell imaging of ECTV- and VACV-infected cells revealed that differences in WV-associated actin comet morphology did not lead to changes in the speed of actin-based motility (Fig. 8B and C; see Videos S1 and S2 in the supplemental material). Although ECTV-induced actin comets were not significantly different in speed from VACV-induced actin comets, there was more speed variation between individual actin comets, with standard deviations of 0.050 μm/s and 0.018 μm/s, respectively. Furthermore, 100% of VACV-induced actin comets visible at the start of imaging persisted for the duration of imaging (1 min 13 s), compared to 28% for ECTV (Fig. 8D).

ECTV ΔA36R is attenuated *in vivo*. Having demonstrated that A36R plays a conserved role in directing the subcellular transport of ECTV, we next examined the effects of disabling this motility on infection of the ECTV-susceptible BALB/c mouse strain, using three different doses of virus. In the group that received the lowest dose (10^2 PFU ECTV), 10 of 15 mice (66%) succumbed to

FIG 2 Actin-based motility of ECTV is via an N-Wasp-dependent pathway. (A) BSC-1 cells were infected with ECTV or VACV at an MOI of 1 and fixed at the indicated time points. Cells were stained with phalloidin and assessed for the presence of actin comets ($n = 50$ per time point, in duplicate). The percentage of cells with actin tails was calculated. Error bars indicate standard errors. (B) HeLa cells were infected with ECTV or VACV, fixed, and stained for immunofluorescence assays with anti-B5 (NPC) (red) or phalloidin (green). Arrowheads indicate a WV associated with an actin comet. ECTV-infected cells were also probed with anti-B5 (NPC) (red), anti-A36-Y112 (green), and DAPI (blue) (C) or with phalloidin (red), an antiphosphotyrosine antibody (4G10; green), and DAPI (blue) (D). (E) N-Wasp$^{-/-}$ MEFs were mock transfected or transfected with an N-Wasp-GFP expression vector (green). At 24 h posttransfection, cells were infected with ECTV and fixed. For immunofluorescence assays, fixed cells were stained with phalloidin (red) and DAPI (blue). Arrowheads indicate WV (C) or WV associated with an actin comet (D and E). Bars, 10 μm.

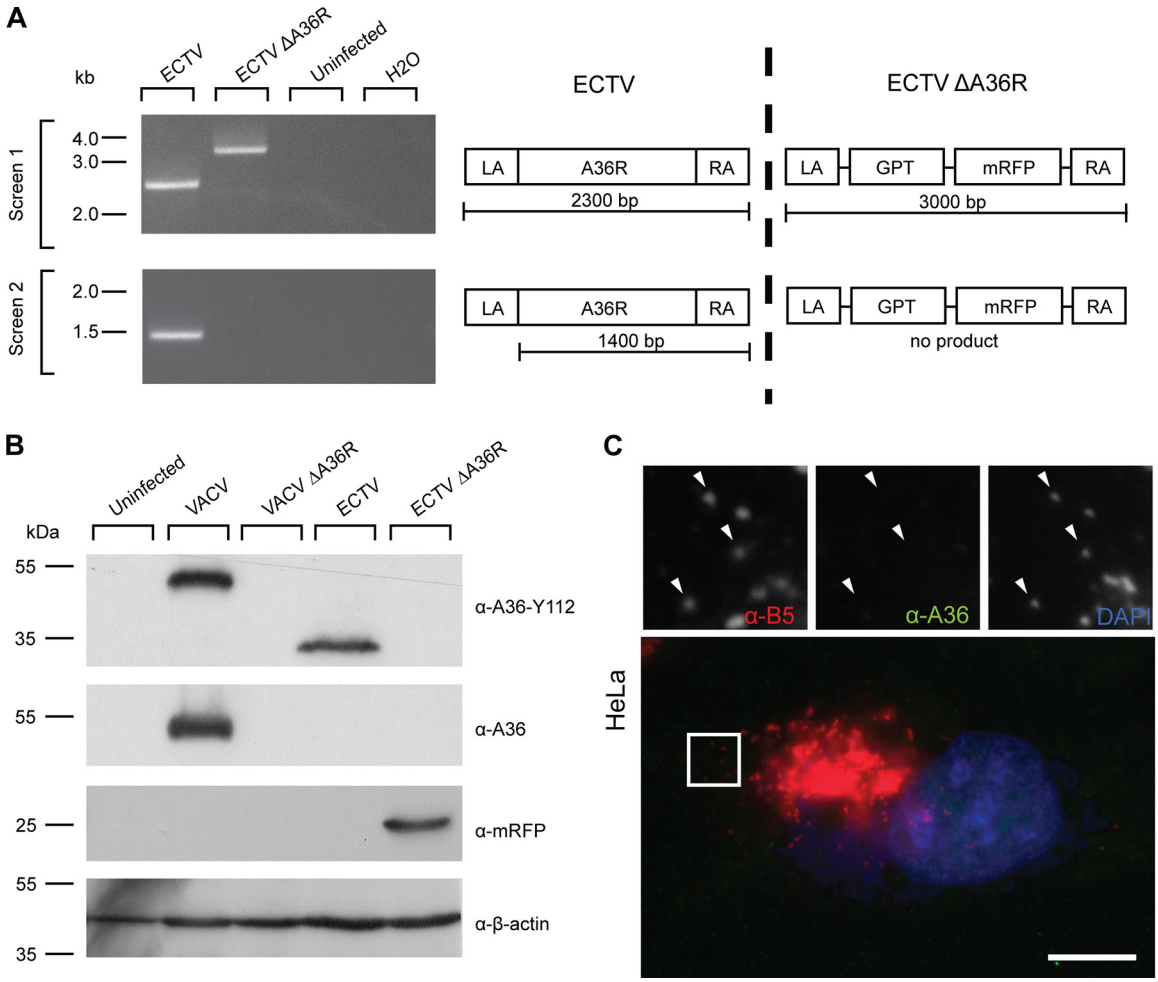

FIG 4 Construction and verification of ECTV ΔA36R. (A) BSC-1 cells were infected with ECTV or recombinant ECTV ΔA36R, and cell lysates were collected at 48 hpi. Genomic DNA was extracted and PCR conducted with two primer pairs, a36r.lafor-a36r.rarev and a36r.for-a36r.raev, to confirm deletion of A36R and insertion of the selection cassette. Uninfected cell lysate genomic DNA and a no-template control were run simultaneously as negative controls. Molecular size markers are indicated on the left. A schematic of the PCRs performed is represented on the right. (B) BSC-1 cells were infected with VACV, VACV ΔA36R, ECTV, or ECTV ΔA36R at an MOI of 1, and cell lysates were collected at 16 hpi (VACV) or 48 hpi (ECTV). Cell lysates were separated by SDS-PAGE and transferred to nitrocellulose membranes for immunoblotting with anti-A36 (raised against the C terminus of VACV A36, which is absent in ECTV A36), anti-A36-Y112, anti-mRFP, and anti-β-actin (as a loading control). Molecular size markers are indicated on the left. (C) HeLa cells were infected with ECTV ΔA36R, fixed, and stained for immunofluorescence assays with anti-B5 (NPC) (red), anti-A36-Y112 (green), and DAPI (blue). Arrowheads indicate WV. Bar, 10 μm.

mousepox and died by 18 dpi (Fig. 9A). Mice that survived past day 18 developed pox lesions on their tails that ulcerated with time, and they were therefore euthanized at 28 dpi for ethical reasons. Animals in the groups infected with 10^3 ($n = 7$) and 10^4 PFU ($n = 6$) of ECTV succumbed to mousepox with 100% mortality, with mean times to death of 11.1 and 8.8 days, respectively. All mice infected with ECTV had an unkempt hair coat and hunched posture from about 6 dpi and generally became moribund before they died. In contrast, mice infected with the 3 different doses of ECTV ΔA36R survived until at least 33 dpi (Fig. 9A), with no overt clinical signs of disease. Organism-wide dissemination of virus was clearly affected by deletion of A36R. The viral loads in the draining lymph nodes, spleen, and liver at 5 dpi were 3 to 4 $\log_{10}$ PFU higher in mice infected with 10^2 PFU ECTV than in those infected with ECTV ΔA36R (Fig. 9B). This difference further increased to 5 $\log_{10}$ PFU at 8 dpi, due to the increasing viral loads in all organs of ECTV-infected mice and decreasing viral loads in all organs of ECTV ΔA36R-infected mice (Fig. 9C). While ECTV infection is lethal in BALB/c mice, ECTV ΔA36R infection is readily controlled, showing strong attenuation *in vivo*. This attenuation was also evident in ECTV-resistant C57BL/6 wild-type mice (data not shown) and C57BL/6 Rag-$1^{-/-}$ mice, which lack B and T cells and therefore do not possess adaptive immunity (Fig. 9D). Titers of ECTV ΔA36R were 1 to 4 $\log_{10}$ PFU lower than those of ECTV at 5 dpi. We were unable to determine viral loads in organs of Rag$1^{-/-}$ mice at 8 dpi, as all mice infected with ECTV had died by this time, whereas those infected with ECTV ΔA36R were still alive, with no clinical signs of disease.

The finding that ECTV ΔA36R titers were significantly lower than those of ECTV early during the course of infection, even in C57BL/6 Rag-$1^{-/-}$ mice, suggested that either the virus replicated poorly *in vivo* or the innate immune system effectively controlled virus replication. Since NK cells play a key role in controlling ECTV replication early in infection and are activated rapidly fol-

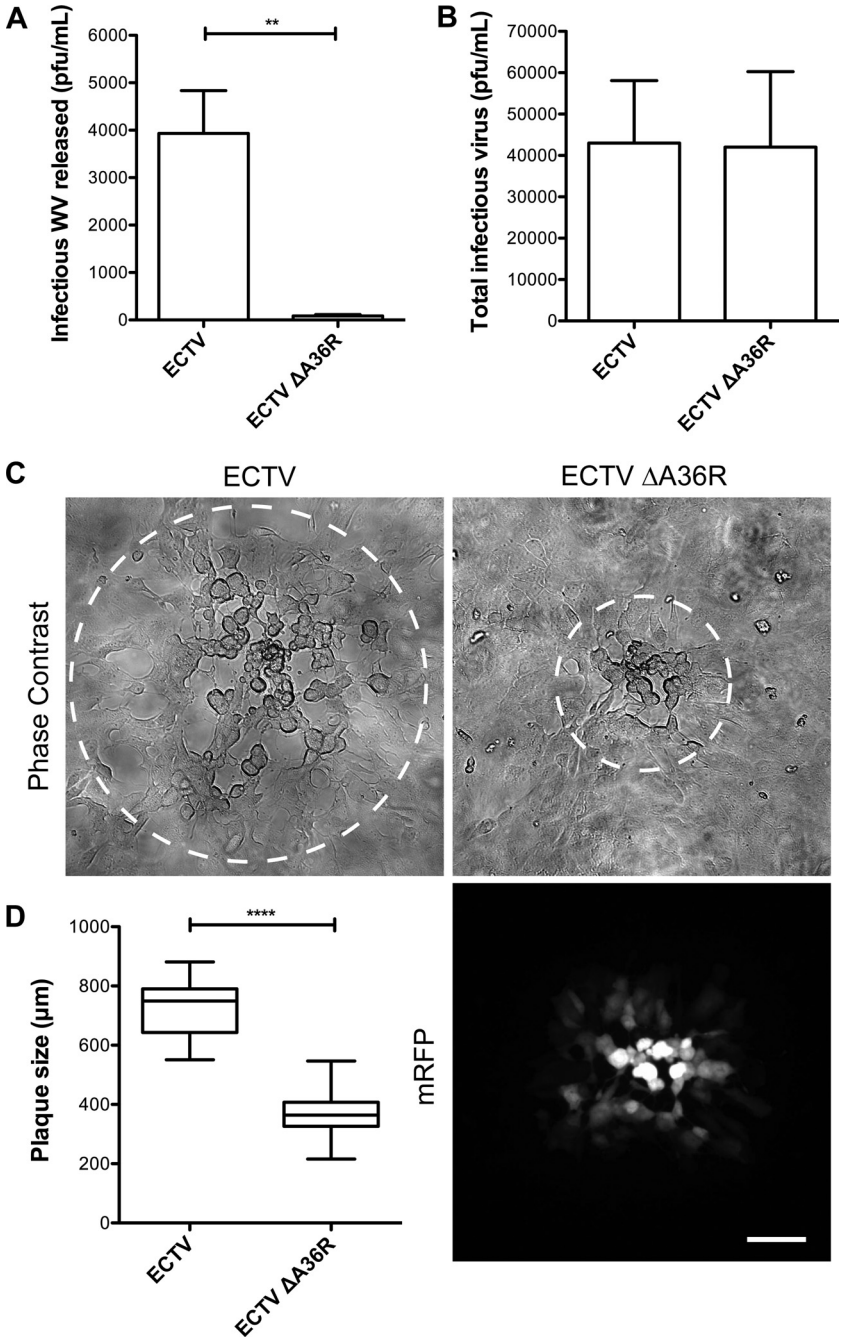

FIG 5 Deletion of ECTV A36R results in reduced WV release and reduced virus spread. BSC-1 cells were infected with ECTV or ECTV ΔA36R at an MOI of 0.1, and supernatants were collected at 32 hpi and centrifuged at 6,000 rpm for 10 min to remove cells and cellular debris (A), or all cells were scraped into supernatants at 16 hpi before undergoing three freeze-thaw cycles to release viruses (B). Plaque assays were then performed with BSC-1 monolayers overlaid with 1.5% CMC-DMEM and stained at 5 dpi with crystal violet to quantify plaques. Differences between ECTV and ECTV ΔA36R were statistically different ($P = 0.0018$; unpaired t test) for infectious WV released but not for total infectious virus. (C) BSC-1 cell monolayers were infected with ECTV or ECTV ΔA36R and overlaid with 1.5% CMC-DMEM. At 4 dpi, plaques were visualized by phase-contrast microscopy (top panels) and fluorescence microscopy (bottom right panel). Bar, 100 μm. (D) The diameter of each plaque was determined in ImageJ 1.4.4 as the widest point at which cytopathic effects were observed (circled in panel C). Data for three experimental replicates were pooled ($n = 30$). Data for VACV and ECTV were statistically different ($P < 0.0001$; unpaired t test).

lowing ECTV infection (7, 24, 49), we assessed the cytolytic activity of NK cells in virus-infected BALB/c and C57BL/6 wild-type mice at 5 dpi, the peak of the NK cell response. The NK cell activity induced by ECTV ΔA36R was >3-fold lower in BALB/c mice (Fig. 9E), and at least 27-fold lower in C57BL/6 mice (Fig. 9F), than the activity that was generated by ECTV infection in both strains of mice. The data suggested that it is unlikely that NK cells contribute to the early control of mutant virus replication.

ECTV ΔA36R infection induces protective immunity. We determined whether ECTV ΔA36R, which replicated poorly in

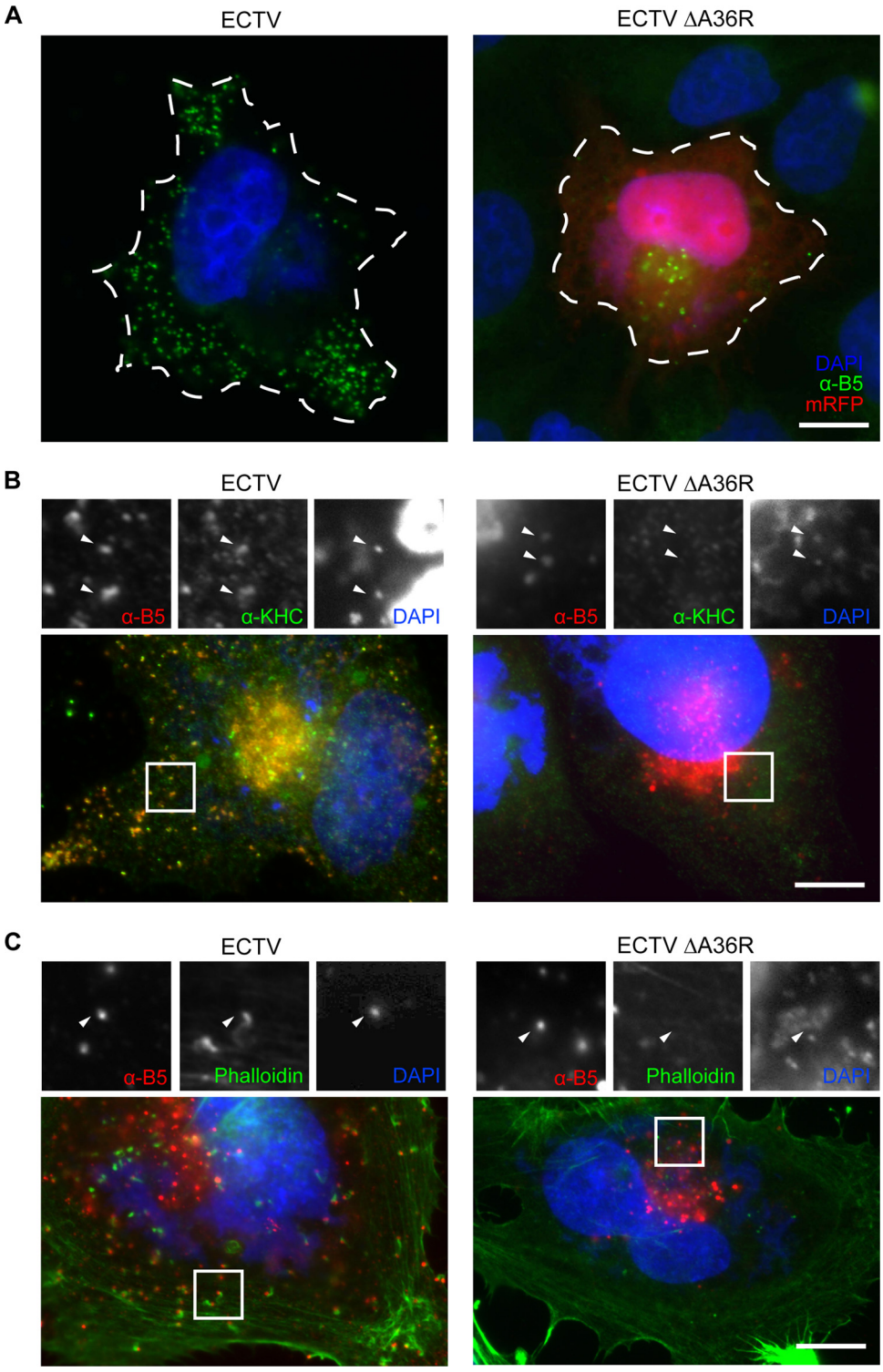

FIG 6 Deficient actin- and microtubule-based motility of ECTV ΔA36R. (A) HeLa cells were infected with ECTV or ECTV ΔA36R, fixed, and probed in immunofluorescence assays with anti-B5 (NPC) (green) and DAPI (blue). The dotted line shows the cell periphery as determined by phase-contrast microscopy. Infected cells were also probed with anti-B5 (NPC) (red), KHC antiserum (green), and DAPI (blue) (B) or with anti-B5 (NPC) (red), phalloidin (green), and DAPI (blue) (C). mRFP expressed by ECTV ΔA36R was bleached by the addition of a high concentration of *p*-phenylenediamine (1% [wt/vol]) to the mounting solution. Arrowheads indicate WV. Bars, 10 μm.

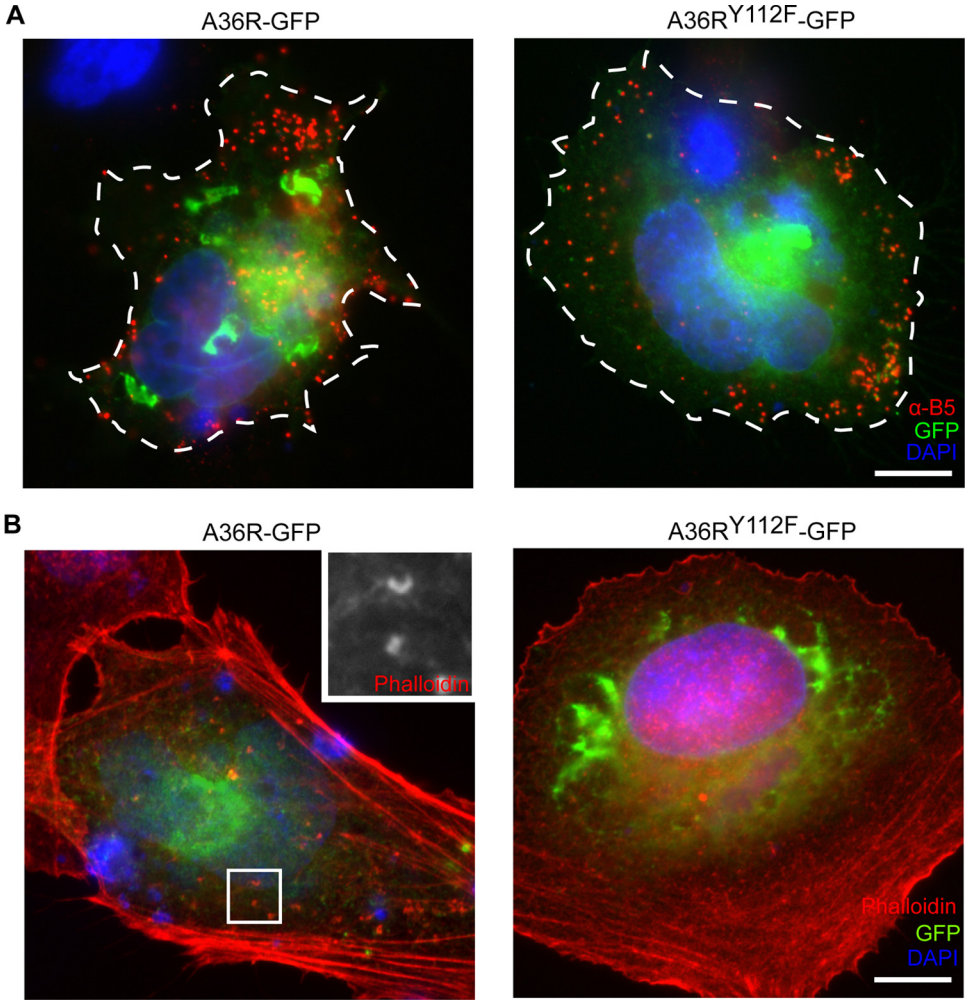

FIG 7 Transport defects of ECTV ΔA36R are restored by transient A36 expression. (A) HeLa cells were infected with ECTV ΔA36R and transfected with plasmid constructs for A36R-GFP and A36Y112F-GFP (green) for transient expression under the control of pE/L, fixed, and then stained for immunofluorescence assays with anti-B5 (NPC) (red) and DAPI (blue). The dotted line indicates the cell periphery as determined by phase-contrast microscopy. (B) Infected and transfected cells were also probed with phalloidin (red) and DAPI (blue). Bars, 10 μm.

mice, induced any protective immunity to ECTV. All mice that had survived infection with either 10^2, 10^3, or 10^4 PFU ECTV ΔA36R were challenged with a lethal dose (10^4 PFU) of ECTV at 33 dpi. Eight days later, mice were sacrificed, and spleens, livers, and lymph nodes were collected for determination of viral loads, whereas sera were used to measure anti-ECTV antibody titers. Splenocytes were used to measure the recall anti-ECTV-specific CTL response.

Virus was below the level of detection in the spleen, liver, and lymph nodes in mice challenged with a lethal dose of ECTV (data not shown), indicating that a primary infection with all 3 doses of ECTV ΔA36R induced protective immunity against a subsequent lethal virus challenge. Recall anti-ECTV CTL responses were generated in all groups, at near comparable levels in magnitude (Fig. 10A).

Since antibody plays a critical role in recovery and virus control during both primary and secondary ECTV infections (47, 48), we measured virus-specific antibodies in sera obtained from mice infected with ECTV ΔA36R during primary infection and subsequent secondary challenge. ECTV-specific IgG was clearly induced during primary (14 and 28 dpi) infection with ECTV ΔA36R and 8 days after challenge with ECTV (Fig. 10B). Antibody titers were augmented as the virus inoculum dose was increased. It was also evident that as the antibody response matured over time (i.e., between 14 and 28 dpi), the anti-ECTV IgG titers also increased. In addition, IgG titers were boosted further in all groups following secondary virus challenge. ECTV ΔA36R generated neutralizing antibodies during primary infection, and neutralizing titers increased substantially after the secondary virus challenge (Fig. 10C).

DISCUSSION

The ECTV (Moscow) genome is highly conserved between related members of the orthopoxvirus genus, with approximately 90 to 99% identity at the amino acid level for WV-specific proteins (8). Our analysis of ECTV replication suggests that the morphogenesis pathway that gives rise to WV is also conserved. A subset of MV generated at the virus factory acquire B5 and A36 immunoreactivity and are transported to the cell periphery in a microtubule-dependent manner. We observed a delay in the replication of ECTV *in vitro*, compared to that of VACV (Western Reserve), that

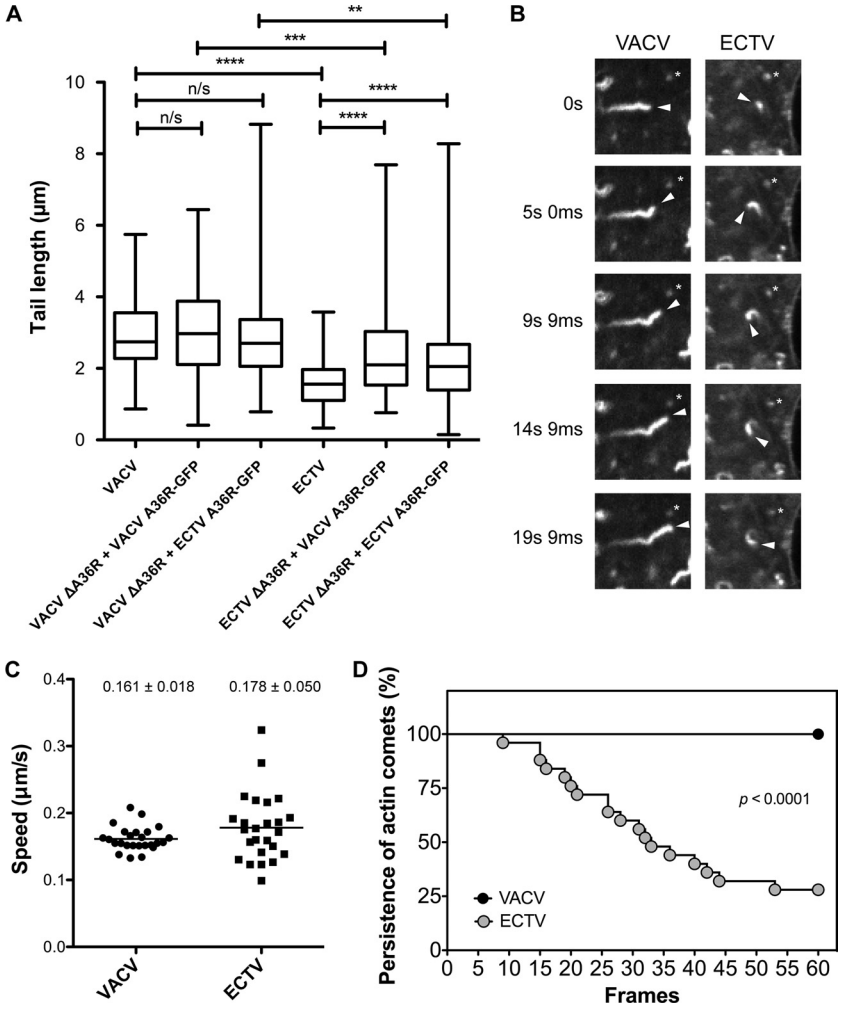

FIG 8 Characteristics of ECTV actin-based motility. (A) BSC-1 cells were infected with VACV WR, VACV ΔA36R, ECTV Mos, or ECTV ΔA36R and transfected with a plasmid construct encoding VACV A36R-GFP or ECTV A36R-GFP for transient expression under the control of pE/L. Cells were fixed and stained for immunofluorescence assays with anti-B5 (NPC) (blue) and phalloidin (red) to visualize actin tails. Tail lengths of six actin tails from at least six different cells in three experimental replicates ($n = 118$) were measured in ImageJ 1.4.4 and pooled. There were significant differences in tail lengths by the unpaired *t* test: n/s, not significant; **, $P < 0.005$; ***, $P < 0.001$; and ****, $P < 0.0001$. (B) HeLa cells were infected with VACV or ECTV, transfected with pE/L Lifeact-GFP, and imaged at 8 to 10 hpi (VACV) or 24 to 26 hpi (ECTV). Arrowheads indicate the tips of actin comets, and asterisks indicate stationary objects. (C) Average speeds of 5 actin comets in 5 different cells ($n = 25$), calculated over 6 consecutive frames (3.7 s apart) by use of the Manual Tracker plug-in in ImageJ. (D) Number of frames in which 5 actin comets in 5 different cells ($n = 25$) visibly persisted over 60 consecutive frames (1.2 s apart) of image acquisition. Data for VACV and ECTV were statistically different ($P < 0.0001$; log rank [Mantel-Cox] test).

was independent of the cell type and origin of host cells. The difference in replication dynamics may reflect adaptation by VACV to replication in cultured cells, as this delay is not apparent *in vivo*, where infection of mice with either VACV or ECTV is lethal at 6 to 8 days postinfection (51). This interpretation is complicated by the absence of a known native host for VACV and by differences in the virus titer used to achieve a lethal dose.

Through immunoblot analyses, we observed that like VACV A36, ECTV A36 has an early component to its expression profile, and alignments of the promoter region up to 100 nucleotides upstream of the open reading frames of the two genes showed 98% identity. The early expression of VACV A36 is believed to be important in repulsion of superinfecting virions, a process which allows viral spread to occur at a rate beyond the speed of its replicative cycle (13). Through cell surface signaling, viral entry into already infected cells is blocked, and superinfecting virions are directed toward uninfected cells (13). Our results show that because ECTV A36 is expressed early, it is possible that repulsion of superinfecting virions also occurs with ECTV.

We have shown that the viral protein ECTV A36 plays a key role in mediating subcellular transport of ECTV, as shown previously for VACV A36 during VACV replication (26, 32, 51, 74, 75). Divergent orthopoxviruses appear to encode functional homologues of A36 at conserved genomic loci, and while these are highly conserved at the N terminus, they lack significant sequence conservation (8 to 15% amino acid identity) at the C terminus (52). ECTV A36 is consistent in displaying greater diversity at the C terminus, in fact possessing the greatest extent of divergence among all available orthopoxvirus genomes with its predicted 63-residue C-terminal truncation.

Immunoblot analysis confirmed that ECTV A36R encodes a truncated protein. Nonetheless, the protein retains the essential

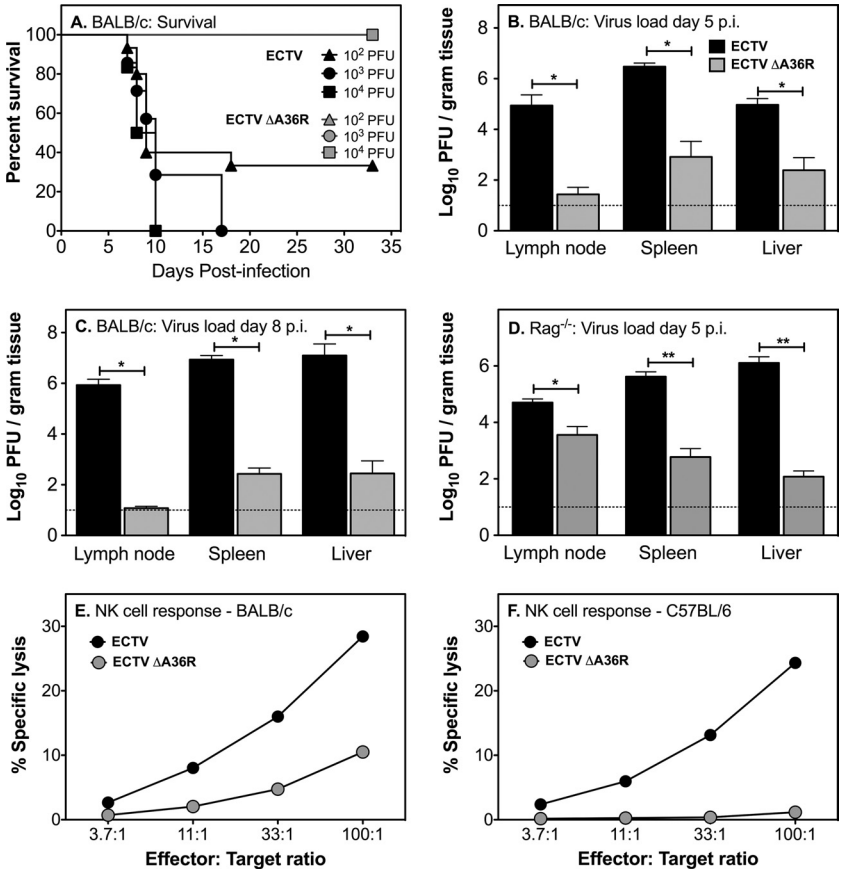

FIG 9 Virulence of ECTV ΔA36R in mouse infections. Groups of 6 to 15 female BALB/c mice were infected subcutaneously in the left hind leg with 10^2, 10^3, or 10^4 PFU ECTV or ECTV ΔA36R. (A) Mice were bled at 0, 14, and 28 dpi to measure antibody titers in sera (see Fig. 10) and monitored for survival over 33 days. There were significant differences in survival of mice infected with mutant virus or WT virus ($P < 0.0001$ at 10^2 and 10^3 PFU and $P < 0.001$ at 10^4 PFU; log rank [Mantel-Cox] test). Data shown for the 10^2 dose of virus were combined from two different experiments. Separate groups of mice were infected with 10^2 PFU of virus and euthanized at 5 (B) or 8 (C) dpi, and the viral loads in lymph nodes, spleens, and livers were quantified by viral plaque assays. (D) Groups of 5 Rag-$1^{-/-}$ female mice were infected with 10^3 PFU ECTV or ECTV ΔA36R and euthanized at 5 dpi, and the viral loads in lymph nodes, spleens, and livers were quantified by plaque assays. Titers of ECTV and ECTV ΔA36R in lymph nodes, livers, and spleens were significantly different by the Mann-Whitney test. *, $P < 0.05$; **, $P < 0.01$. Data shown in panels B, C, and D are mean viral loads with standard errors of the means (SEM). The horizontal dotted lines indicate the limit of detection of the viral plaque assay, which is 1 $\log_{10}$ PFU. Splenic NK cell responses were measured by ^{51}Cr release assay for groups of three BALB/c (E) and C57BL/6 (F) mice that been infected with 10^3 PFU of WT or mutant virus.

transport functions of VACV A36 and possesses microtubule-based motility (Fig. 6 and 7). These observations are in agreement with a previous study in which microtubule transport of WV was rescued in a VACV ΔA36R strain by the expression of the transmembrane domain fused to $A36^{71–100}$, suggesting that a KLC binding site lies within this region (57). This was further supported with yeast two-hybrid assays demonstrating that $A36^{81–100}$ was sufficient to mediate binding to KLC (74). In a recent study, kinesin-1 recruitment was narrowed down to a bipartite tryptophan motif at residues 64 and 65 (WE) and residues 97 and 98 (WD) of VACV A36 (15). While ECTV A36 is conserved at the WD site, it has an amino acid substitution of another acidic residue at the WE site, creating a second WD site. Even though the sites are not absolutely conserved, a bipartite tryptophan domain is retained. In their study, Dodding and colleagues demonstrated that substitution of the WE/WD bipartite tryptophan motif with a WD/WD motif from calsytenin rescues kinesin-1 recruitment, and this substitution is unlikely to have any deleterious effects on microtubule-based motility. ECTV WV particles were still found to partially colocalize with both components of the kinesin-1 motor complex, i.e., KHC and KLC (Fig. 6B and data not shown), suggesting that microtubule transport of WV is likely to operate via a conserved mechanism during ECTV replication.

Furthermore, although the exact role of F12 in microtubule motility of VACV remains to be clarified, evidence suggests that it may mediate or stabilize the binding of A36 to kinesin-1 (14, 35, 41, 72), as yeast two-hybrid screens have identified a specific interaction between $F12^{351–458}$ and $A36^{91–111}$ (14, 35, 41, 72). ECTV Mos possesses a highly conserved homolog of VACV WR F12 (96.69% identity) that bears only two amino acid substitutions, in the region of residues 350 to 457, which may further suggest a conserved mechanism of microtubule-based motility.

Actin-based motility has been observed across the orthopoxvirus genus, in VACV (9), ECTV (2, 4, 22; this study), VARV, and monkeypox virus (55), as well as in more distantly related poxviruses, such as myxoma virus (19) and Yaba-like disease virus (17, 19, 37). In the closely related orthopoxviruses, the nucleation of actin filaments is likely mediated by homologues of VACV A36, as

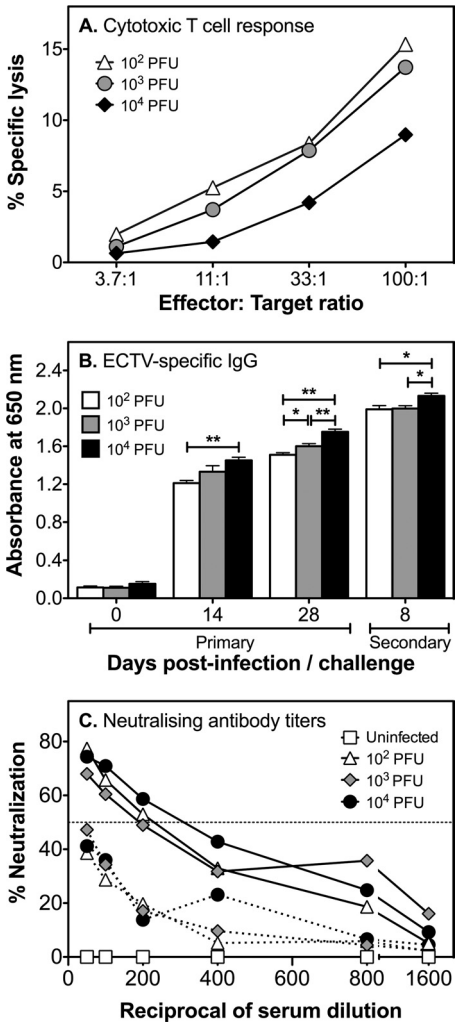

FIG 10 ECTV ΔA36R infection induces protective immunity. At 33 dpi, all BALB/c mice inoculated with 10^2, 10^3, or 10^4 PFU ECTV ΔA36R that survived were challenged with a lethal dose of ECTV by the subcutaneous route. Mice were sacrificed at day 8 postchallenge, and sera, spleens, livers, and lymph nodes were collected. (A) Recall CTL responses in the spleen were similar for all groups. (B) ECTV-specific IgG in serum was measured by ELISA during primary infection (0, 14, and 28 dpi) and 8 days after secondary challenge. ECTV-specific IgG titers increased with increased doses of virus inoculum over time postinfection and after secondary challenge. *, $P < 0.05$; **, $P < 0.01$ (Mann-Whitney test). (C) Serial dilutions of sera, starting at a 1:50 dilution, were performed for mice during primary infection with various doses of ECTV ΔA36R (broken lines) and after secondary challenge with ECTV (solid lines) and were used to determine neutralizing activity. ECTV ΔA36R induced neutralizing antibody during primary infection, though the levels were below the 50% neutralizing titer (horizontal dotted line). Virus was not detected in any of the organs following a secondary virus challenge (data not shown).

we have demonstrated for ECTV. Significantly, ECTV A36 is also the only orthopoxvirus homologue to lack the second tyrosine (Tyr 132) (52); nonetheless, ECTV A36 is sufficient to promote actin-based motility in ECTV and VACV (data not shown). Interestingly, although the more divergent poxviruses do not carry A36 orthologues, the genomic locus where functional actin nucleators are encoded is conserved (17). This study is only the third report defining the loss of actin-based motility in a recombinant virus deleted for the viral nucleator, along with VACV and baculovirus (28, 45).

We observed that ECTV-induced actin comets were morphologically distinct from those present during VACV infection, as they were shorter, and this difference was independent of the time point examined. The obvious explanation for these findings was the absence of the Grb2 binding site (Tyr 132), which when mutated to Phe blocks phosphorylation and Grb2 recruitment and results in shorter actin tails, increased virus motility, and faster N-Wasp turnover (64, 77). However, although they were shorter, ECTV-induced actin comets were not faster than VACV-induced actin comets. This inconsistency was clarified through cross-rescue experiments with GFP-tagged VACV A36 and ECTV A36. Although ECTV ΔA36R rescued with either construct led to tails that were statistically longer than those of ECTV, this was likely an artifact of transient expression and still resulted in shorter tails than those produced by VACV ΔA36R rescued with the same constructs. This established that the identity of the infecting virus, not the nucleator, is responsible for the distinct actin comet morphology. Infection with orthopoxviruses leads to disruption of many host signaling pathways that could conceivably impact actin dynamics within the cell. Although there are a number of cellular proteins that are known to affect pathogen actin comet length, for example, profilin during *Listeria* motility (30), elucidation of the mechanism that defines the different rates of actin nucleation between VACV and ECTV must await future studies.

The reduced microtubule transport and loss of virus-associated actin comets due to disruption of A36R function in ECTV had a significantly attenuated phenotype *in vivo* in two susceptible strains of mice. First, the ECTV-susceptible BALB/c mouse strain did not exhibit any clinical signs of disease and survived doses of ECTV ΔA36R that were otherwise fatal. ECTV ΔA36R titers were several orders of magnitude lower in the draining lymph nodes, spleen, and liver than titers of ECTV at 5 and 8 dpi. Second, ECTV ΔA36R was also attenuated in Rag-$1^{-/-}$ mice, which are devoid of an adaptive immune system. Viral loads in organs of this strain were also orders of magnitude lower than titers of ECTV at 5 dpi. All Rag-$1^{-/-}$ mice infected with ECTV died from the infection by 8 dpi, whereas those infected with ECTV ΔA36R were still alive, with no clinical signs of disease (data not shown). Although we envisage that Rag-$1^{-/-}$ mice would have eventually succumbed to infection with the mutant virus, since adaptive immunity is essential for complete recovery (6, 7), this finding further attests to the importance of microtubule transport and actin-based motility for virus replication, spread, and ability to cause disease.

The BALB/c strain normally generates a poor immune response to ECTV infection, and depending on the virus dose, mice of this strain succumb to mousepox at 7 to 20 dpi (Fig. 9A) (7, 61). However, when infected with mutant viruses lacking thymidine kinase activity (48) or immune evasion molecules that target interferon function (61, 79), they are able to generate an antiviral immune response and recover. Thus, reducing the level of virus replication can tip the balance in favor of the BALB/c mouse, allowing it sufficient time to mount CTL and antibody responses to overcome an infection that is otherwise lethal.

The NK cell response to ECTV infection generally peaks by 5 dpi and contributes to early virus control (7, 24, 49). We reasoned that replication of ECTV ΔA36R was possibly controlled by NK cells, as mutant virus titers were at least 1 to 4 $\log_{10}$ PFU lower than those of ECTV at 5 dpi. However, infection of ECTV-susceptible BALB/c or ECTV-resistant C57BL/6 mice with the mutant virus induced very weak NK cell cytolytic activity that was severalfold

lower than the activity generated by ECTV in both mouse strains. Although a role for other innate cell types in rapidly reducing mutant virus titers cannot be excluded, we believe that the attenuated phenotype of this virus, in contrast to some other ECTV mutants discussed above, is due to its inability to spread efficiently as a consequence of defective subcellular transport.

Although we did not measure the primary CTL response in BALB/c mice infected with ECTV ΔA36R, it is very likely that cell-mediated immunity contributed to the recovery from primary infection (7). Anti-ECTV antibody was clearly generated during primary infection (Fig. 10B), and this response is vital for complete recovery from a primary infection.

Despite the significant attenuation of ECTV ΔA36R, it nonetheless induced protective immunity. BALB/c mice that had recovered from infection with 3 different doses of ECTV ΔA36R were protected against challenge with a lethal dose of ECTV. At day 8 postchallenge, we were unable to demonstrate the presence of virus in all organs examined. Recall CTL (Fig. 10A) and antibody (Fig. 10B and C) responses were clearly generated and were indicative of induction of T and B cell memory during primary infection. Although a role for cell-mediated immunity cannot be excluded completely, humoral immunity is known to absolutely be required for recovery from a secondary orthopoxvirus infection. We have previously shown that humoral immunity, but not the function of CD4 or CD8 T lymphocyte subsets, is required to control virus replication during the acute phase of a secondary ECTV infection (47, 48). This requirement for antibody is not unique to ECTV, as elimination of CD4 or CD8 T cells does not affect monkeypox virus clearance or the neutralizing antibody response during the acute phase of a secondary infection in VACV-vaccinated macaques (20). The findings in the current study suggest that orthopoxvirus vectors with A36 deletions may be considered safe vaccine candidates. A36 deletions generate virions expressing all envelope proteins, so while they have defective transmission and are severely attenuated, all neutralizing epitopes are present in their natural state.

This is the first ECTV recombinant virus with a WV-specific open reading frame deleted. The significant reduction in the capacity of mutant virus to spread locally and be transmitted to other tissues *in vivo* highlights the importance of infective WV and the specific roles played by A36 in subcellular transport. Deletion of genes encoding WV-specific proteins in VACV, such as A36, B5, and A34, also lead to highly attenuated infections in mice (21, 38, 51, 71). The intranasal route of inoculation used in most of these studies mimics large-droplet transmission of smallpox in humans, leading to a systemic disease that shares similarities with smallpox disease progression (3, 46, 50). However, intranasal infection of mice with VACV WR requires large doses (10^4 to 10^6 PFU) to achieve substantial mortality (21, 38, 51), which may not be reflective of the doses of variola virus required to cause disease and death in humans. Using lower infectious doses (10^{-2} to 10^{-4} PFU), we have shown that deletion of A36R in ECTV attenuates the virus to the extent that even genetically susceptible mice are able to survive the infection and generate immunological memory. Our characterization of the role and function of A36R with a combination of a host and its natural pathogen offers considerable advantages toward elucidating its contribution to virulence.

Subcellular transport pathways are critical steps in the replication of many viruses, particularly large DNA viruses, which are significantly hindered by the host cytoplasm environment (69). Recruitment of cellular microtubule motors during virus egress is often complex, requiring multiple, redundant interactions with surface viral proteins. These surface viral proteins are often pleiotropic and possess key roles in other stages of morphogenesis, obfuscating straightforward genetic analysis of their functions in transport. For example, egress of herpes simplex virus 1 (HSV-1) requires kinesin-1 function, and while HSV-1 tegument proteins pUL36 (VP1/2) and pUL37 are good candidate interaction partners (53), null mutants do not produce enveloped virions (10, 11). The effects of these mutations on kinesin-1 recruitment therefore cannot be analyzed effectively, and in fact, no mutations in HSV-1 have been identified that mimic the loss of kinesin-1 function (12, 16). Similarly, ablation of kinesin-2 function blocks Kaposi's sarcoma-associated herpesvirus release, and while the viral protein ORF45 has been shown to interact with kinesin-2 through yeast two-hybrid screens, null mutants again are morphologically defective (63, 80).

In contrast, the microtubule-dependent egress of VACV is mediated by the well-defined interaction between A36 and the kinesin-1 complex, whose disruption produces a strong defect in virus transport but not other aspects of virus morphogenesis. We have exploited this knowledge and translated it to the related virus ECTV to demonstrate that movement on microtubules and polymerized actin is essential for virus propagation and transmission in its natural host. In an intact animal, cell-to-cell virus transmission occurs in a complex three-dimensional environment of tissue. This is distinct from the predominantly two-dimensional surface imposed by virus cell culture techniques such as plaque assays, where virus spread occurs within a cell monolayer and which may overstate the importance of cytoplasmic transport. Our results confirm that cytoplasmic transport is a fundamental barrier to orthopoxvirus transmission in an intact host and therefore an attractive target for inhibiting viral pathogenesis.

ACKNOWLEDGMENTS

We thank Niki Scaplehorn for characterization of the A36-Y112 antibody.

This work was supported by the National Health and Medical Research Council (NHMRC) of Australia (project grant 632785) and The Australian Research Council Federation Discovery Project (DP1096623).

The contents of the published material are solely the responsibility of the individual authors and do not reflect the views of the NHMRC.

REFERENCES

1. **Arakawa Y, Cordeiro JV, Schleich S, Newsome TP, Way M.** 2007. The release of vaccinia from infected cells requires RhoA-mDia modulation of cortical actin. Cell Host Microbe **1**:227–240.
2. **Boratynska A, et al.** 2010. Contribution of rearranged actin structures to the spread of ectromelia virus infection in vitro. Acta Virol. **54**:41–48.
3. **Buller RM.** 2004. Mousepox: a small animal model for biodefense research. Appl. Biosaf. **9**:10–19.
4. **Butler-Cole C, et al.** 2007. An ectromelia virus profilin homolog interacts with cellular tropomyosin and viral A-type inclusion protein. Virol. J. **4**:76.
5. **Chakrabarti S, Sisler JR, Moss B.** 1997. Compact, synthetic, vaccinia virus early/late promoter for protein expression. Biotechniques **23**:1094–1097.
6. **Chaudhri G, Panchanathan V, Bluethmann H, Karupiah G.** 2006. Obligatory requirement for antibody in recovery from a primary poxvirus infection. J. Virol. **80**:6339–6344.
7. **Chaudhri G, et al.** 2004. Polarized type 1 cytokine response and cell-mediated immunity determine genetic resistance to mousepox. Proc. Natl. Acad. Sci. U. S. A. **101**:9057–9062.
8. **Chen N, et al.** 2003. The genomic sequence of ectromelia virus, the causative agent of mousepox. Virology **317**:165–186.

9. **Cudmore S, Cossart P, Griffiths G, Way M.** 1995. Actin-based motility of vaccinia virus. Nature **378**:636–638.
10. **Desai P, Sexton GL, McCaffery JM, Person S.** 2001. A null mutation in the gene encoding the herpes simplex virus type 1 UL37 polypeptide abrogates virus maturation. J. Virol. **75**:10259–10271.
11. **Desai PJ.** 2000. A null mutation in the UL36 gene of herpes simplex virus type 1 results in accumulation of unenveloped DNA-filled capsids in the cytoplasm of infected cells. J. Virol. **74**:11608–11618.
12. **Diefenbach RJ, Miranda-Saksena M, Douglas MW, Cunningham AL.** 2008. Transport and egress of herpes simplex virus in neurons. Rev. Med. Virol. **18**:35–51.
13. **Doceul V, Hollinshead M, van der Linden L, Smith GL.** 2010. Repulsion of superinfecting virions: a mechanism for rapid virus spread. Science **327**:873–876.
14. **Dodding M, Newsome TP, Collinson L, Edwards C, Way M.** 2009. An E2-F12 complex is required for IEV morphogenesis during vaccinia infection. Cell. Microbiol. **11**:808–824.
15. **Dodding MP, Mitter R, Humphries AC, Way M.** 2011. A kinesin-1 binding motif in vaccinia virus that is widespread throughout the human genome. EMBO J. **30**:4523–4538.
16. **Dodding MP, Way M.** 2011. Coupling viruses to dynein and kinesin-1. EMBO J. **30**:3527–3539.
17. **Dodding MP, Way M.** 2009. Nck- and N-WASP-dependent actin-based motility is conserved in divergent vertebrate poxviruses. Cell Host Microbe **6**:536–550.
18. **Dohner K, Nagel CH, Sodeik B.** 2005. Viral stop-and-go along microtubules: taking a ride with dynein and kinesins. Trends Microbiol. **13**:320–327.
19. **Duteyrat JL, Gelfi J, Bertagnoli S.** 2006. Ultrastructural study of myxoma virus morphogenesis. Arch. Virol. **151**:2161–2180.
20. **Edghill-Smith Y, et al.** 2005. Smallpox vaccine-induced antibodies are necessary and sufficient for protection against monkeypox virus. Nat. Med. **11**:740–747.
21. **Engelstad M, Smith GL.** 1993. The vaccinia virus 42-kDa envelope protein is required for the envelopment and egress of extracellular virus and for virus virulence. Virology **194**:627–637.
22. **Erez N, et al.** 2009. Induction of cell-cell fusion by ectromelia virus is not inhibited by its fusion inhibitory complex. Virol. J. **6**:151.
23. **Esteban DJ, Buller RM.** 2005. Ectromelia virus: the causative agent of mousepox. J. Gen. Virol. **86**:2645–2659.
24. **Fang M, Lanier LL, Sigal LJ.** 2008. A role for NKG2D in NK cell-mediated resistance to poxvirus disease. PLoS Pathog. **4**:e30. doi:10.1371/journal.ppat.0040030.
25. **Frischknecht F, et al.** 1999. Tyrosine phosphorylation is required for actin-based motility of vaccinia but not Listeria or Shigella. Curr. Biol. **9**:89–92.
26. **Frischknecht F, et al.** 1999. Actin-based motility of vaccinia virus mimics receptor tyrosine kinase signalling. Nature **401**:926–929.
27. **Geada MM, Galindo I, Lorenzo MM, Perdiguero B, Blasco R.** 2001. Movements of vaccinia virus intracellular enveloped virions with GFP tagged to the F13L envelope protein. J. Gen. Virol. **82**:2747–2760.
28. **Goley ED, et al.** 2006. Dynamic nuclear actin assembly by Arp2/3 complex and a baculovirus WASP-like protein. Science **314**:464–467.
29. **Greber UF, Way M.** 2006. A superhighway to virus infection. Cell **124**:741–754.
30. **Grenklo S, et al.** 2003. A crucial role for profilin-actin in the intracellular motility of Listeria monocytogenes. EMBO Rep. **4**:523–529.
31. **Herrero-Martinez E, Roberts KL, Hollinshead M, Smith GL.** 2005. Vaccinia virus intracellular enveloped virions move to the cell periphery on microtubules in the absence of the A36R protein. J. Gen. Virol. **86**:2961–2968.
32. **Hollinshead M, et al.** 2001. Vaccinia virus utilizes microtubules for movement to the cell surface. J. Cell Biol. **154**:389–402.
33. **Hollinshead M, Vanderplasschen A, Smith GL, Vaux DJ.** 1999. Vaccinia virus intracellular mature virions contain only one lipid membrane. J. Virol. **73**:1503–1517.
34. **Huang J, et al.** 2004. The poxvirus p28 virulence factor is an E3 ubiquitin ligase. J. Biol. Chem. **279**:54110–54116.
35. **Johnston SC, Ward BM.** 2009. The vaccinia virus protein F12 associates with IEV through an interaction with A36. J. Virol. **83**:1708–1717.
36. **Karupiah G, Buller RM, Van Rooijen N, Duarte CJ, Chen J.** 1996. Different roles for $CD4^+$ and $CD8^+$ T lymphocytes and macrophage subsets in the control of a generalized virus infection. J. Virol. **70**:8301–8309.
37. **Law M, Hollinshead M, Lee HJ, Smith GL.** 2004. Yaba-like disease virus protein Y144R, a member of the complement control protein family, is present on enveloped virions that are associated with virus-induced actin tails. J. Gen. Virol. **85**:1279–1290.
38. **McIntosh AA, Smith GL.** 1996. Vaccinia virus glycoprotein A34R is required for infectivity of extracellular enveloped virus. J. Virol. **70**:272–281.
39. **Mombaerts P, et al.** 1992. RAG-1-deficient mice have no mature B and T lymphocytes. Cell **68**:869–877.
40. **Moreau V, et al.** 2000. A complex of N-WASP and WIP integrates signalling cascades that lead to actin polymerization. Nat. Cell Biol. **2**:441–448.
41. **Morgan GW, et al.** 2010. Vaccinia protein F12 has structural similarity to kinesin light chain and contains a motor binding motif required for virion export. PLoS Pathog. **6**:e1000785.
42. **Moss B, Shisler JL.** 2001. Immunology 101 at poxvirus U: immune evasion genes. Semin. Immunol. **13**:59–66.
43. **Newsome TP, Scaplehorn N, Way M.** 2004. SRC mediates a switch from microtubule- to actin-based motility of vaccinia virus. Science **306**:124–129.
44. **Newsome TP, Weisswange I, Frischknecht F, Way M.** 2006. Abl collaborates with Src family kinases to stimulate actin-based motility of vaccinia virus. Cell. Microbiol. **8**:233–241.
45. **Ohkawa T, Volkman LE, Welch MD.** 2010. Actin-based motility drives baculovirus transit to the nucleus and cell surface. J. Cell Biol. **190**:187–195.
46. **Panchanathan V, Chaudhri G, Karupiah G.** 2008. Correlates of protective immunity in poxvirus infection: where does antibody stand? Immunol. Cell Biol. **86**:80–86.
47. **Panchanathan V, Chaudhri G, Karupiah G.** 2005. Interferon function is not required for recovery from a secondary poxvirus infection. Proc. Natl. Acad. Sci. U. S. A. **102**:12921–12926.
48. **Panchanathan V, Chaudhri G, Karupiah G.** 2006. Protective immunity against secondary poxvirus infection is dependent on antibody but not on CD4 or CD8 T-cell function. J. Virol. **80**:6333–6338.
49. **Parker AK, Parker S, Yokoyama WM, Corbett JA, Buller RM.** 2007. Induction of natural killer cell responses by ectromelia virus controls infection. J. Virol. **81**:4070–4079.
50. **Parker S, et al.** 2009. Mousepox in the C57BL/6 strain provides an improved model for evaluating anti-poxvirus therapies. Virology **385**:11–21.
51. **Parkinson JE, Smith GL.** 1994. Vaccinia virus gene A36R encodes a M(r) 43–50 K protein on the surface of extracellular enveloped virus. Virology **204**:376–390.
52. **Pulford DJ, Meyer H, Ulaeto D.** 2002. Orthologs of the vaccinia A13L and A36R virion membrane protein genes display diversity in species of the genus Orthopoxvirus. Arch. Virol. **147**:995–1015.
53. **Radtke K, et al.** 2010. Plus- and minus-end directed microtubule motors bind simultaneously to herpes simplex virus capsids using different inner tegument structures. PLoS Pathog. **6**:e1000991. doi:10.1371/journal.ppat.1000991.
54. **Reeves PM, et al.** 2005. Disabling poxvirus pathogenesis by inhibition of Abl-family tyrosine kinases. Nat. Med. **11**:731–739. (Erratum, 11:1361.)
55. **Reeves PM, et al.** 2011. Variola and monkeypox viruses utilize conserved mechanisms of virion motility and release that depend on Abl and SRC family tyrosine kinases. J. Virol. **85**:21–31.
56. **Riedl J, et al.** 2008. Lifeact: a versatile marker to visualize F-actin. Nat. Methods **5**:605–607.
57. **Rietdorf J, et al.** 2001. Kinesin-dependent movement on microtubules precedes actin-based motility of vaccinia virus. Nat. Cell Biol. **3**:992–1000.
58. **Roberts KL, Smith GL.** 2008. Vaccinia virus morphogenesis and dissemination. Trends Microbiol. **16**:472–479.
59. Reference deleted.
60. **Rottger S, Frischknecht F, Reckmann I, Smith GL, Way M.** 1999. Interactions between vaccinia virus IEV membrane proteins and their roles in IEV assembly and actin tail formation. J. Virol. **73**:2863–2875.
61. **Sakala IG, et al.** 2007. Poxvirus-encoded gamma interferon binding protein dampens the host immune response to infection. J. Virol. **81**:3346–3353.
62. **Sanderson CM, Hollinshead M, Smith GL.** 2000. The vaccinia virus A27L protein is needed for the microtubule-dependent transport of intracellular mature virus particles. J. Gen. Virol. **81**:47–58.
63. **Sathish N, Zhu FX, Yuan Y.** 2009. Kaposi's sarcoma-associated herpesvirus ORF45 interacts with kinesin-2 transporting viral capsid-tegument

complexes along microtubules. PLoS Pathog. **5**:e1000332. doi:10.1371/journal.ppat.1000332.
64. **Scaplehorn N, et al.** 2002. Grb2 and Nck act cooperatively to promote actin-based motility of vaccinia virus. Curr. Biol. **12**:740–745.
65. **Schepis A, Stauber T, Krijnse Locker J.** 2007. Kinesin-1 plays multiple roles during the vaccinia virus life cycle. Cell. Microbiol. **9**:1960–1973.
66. **Seet BT, et al.** 2003. Poxviruses and immune evasion. Annu. Rev. Immunol. **21**:377–423.
67. **Smith GL, Symons JA, Khanna A, Vanderplasschen A, Alcami A.** 1997. Vaccinia virus immune evasion. Immunol. Rev. **159**:137–154.
68. **Snapper SB, et al.** 2001. N-WASP deficiency reveals distinct pathways for cell surface projections and microbial actin-based motility. Nat. Cell Biol. **3**:897–904.
69. **Sodeik B.** 2000. Mechanisms of viral transport in the cytoplasm. Trends Microbiol. **8**:465–472.
70. **Taylor MP, Koyuncu OO, Enquist LW.** 2011. Subversion of the actin cytoskeleton during viral infection. Nat. Rev. Microbiol. **9**:427–439.
71. **Tscharke DC, Reading PC, Smith GL.** 2002. Dermal infection with vaccinia virus reveals roles for virus proteins not seen using other inoculation routes. J. Gen. Virol. **83**:1977–1986.
72. **van Eijl H, Hollinshead M, Rodger G, Zhang WH, Smith GL.** 2002. The vaccinia virus F12L protein is associated with intracellular enveloped virus particles and is required for their egress to the cell surface. J. Gen. Virol. **83**:195–207.
73. **van Eijl H, Hollinshead M, Smith GL.** 2000. The vaccinia virus A36R protein is a type Ib membrane protein present on intracellular but not extracellular enveloped virus particles. Virology **271**:26–36.
74. **Ward BM, Moss B.** 2004. Vaccinia virus A36R membrane protein provides a direct link between intracellular enveloped virions and the microtubule motor kinesin. J. Virol. **78**:2486–2493.
75. **Ward BM, Moss B.** 2001. Vaccinia virus intracellular movement is associated with microtubules and independent of actin tails. J. Virol. **75**:11651–11663.
76. **Ward BM, Moss B.** 2001. Visualization of intracellular movement of vaccinia virus virions containing a green fluorescent protein-B5R membrane protein chimera. J. Virol. **75**:4802–4813.
77. **Weisswange I, Newsome TP, Schleich S, Way M.** 2009. The rate of N-WASP exchange limits the extent of Arp2/3 complex dependent actin-based motility. Nature **458**:87–91.
78. **Wilton BA, et al.** 2008. Ectromelia virus BTB/kelch proteins, EVM150 and EVM167, interact with cullin-3-based ubiquitin ligases. Virology **374**:82–99.
79. **Xu RH, et al.** 2008. The orthopoxvirus type I IFN binding protein is essential for virulence and an effective target for vaccination. J. Exp. Med. **205**:981–992.
80. **Zhu FX, Li X, Zhou F, Gao SJ, Yuan Y.** 2006. Functional characterization of Kaposi's sarcoma-associated herpesvirus ORF45 by bacterial artificial chromosome-based mutagenesis. J. Virol. **80**:12187–12196.